공학박사학위논문

Multifunctional and Biocompatible Nanomaterials Based on Multiple Quantum Dots/Iron Oxide Nanoparticles-Embedded Silica Nanosphere

다수의 양자점/산화철 나노입자가 담지된 실리카 나노구체를 기반으로 한 다기능성 생체 친화성 나노물질에 관한 연구

2016년 2월

서울대학교 대학원

화학생물공학부

경 산

Multifunctional and Biocompatible Nanomaterials Based on Multiple Quantum Dots/Iron Oxide Nanoparticles-Embedded Silica Nanosphere

다수의 양자점/산화철 나노입자가 담지된 실리카 나노구체를 기반으로 한 다기능성 생체 친화성 나노물질에 관한 연구

지도 교수 이 윤 식

이 논문을 공학박사학위논문으로 제출함
2016년 2월
서울대학교 대학원
화학생물공학부
경 산

경산의 공학박사학위논문을 인준함
2015년 11월

위 원 장 _____ (인)

부위원장 _____ (인)

위 원 _____ (인)

위 원 _____ (인)

위 원 _____ (인)

ABSTRACT

Multifunctional and Biocompatible Nanomaterials Based on Multiple Quantum Dots/Iron Oxide Nanoparticles-Embedded Silica Nanosphere

San Kyeong

School of Chemical and Biological Engineering

The Graduate School

Seoul National University

Quantum dots (QDs) and superparamagnetic Fe_3O_4 nanoparticles (NPs) have garnered considerable attention in biomedical applications. Novel surface modification strategy could enhance the performance of those NPs.

In chapter 1, silica-coated, QD–embedded silica NPs (QD-SiO_2 NPs) containing QDs composed of CdSe@CdS@ZnS were prepared and the structure based advantages were compared with single QD having similar QY. These QD-SiO_2 NPs exhibited *ca.* 200 times stronger photoluminescence (PL) than single QDs. Cytotoxicity studies revealed that QD-SiO_2 NPs were less toxic than equivalent numbers of silica-free

single QDs. The excellence of QD-SiO_2 NPs with regard to in vitro applications was illustrated by significantly enhanced fluorescence signals from QD-SiO_2 NPs internalized cancer cells and stem cells.

In chapter 2, QD-assembled silica NPs bearing a polydiacetylene (PDA) supramolecules on their surface (PDA-QD-SiO_2 NPs) were described. The resulting PDA-QD-SiO_2 NPs showed discrete QD photoluminescence for encoding as well as PDA fluorescence for sensing a target without interference or overlap. Under heating stress of the PDA-QD-SiO_2 NPs, the color of the PDA changed from blue to red, which also allowed us to observe the fluorescence emitted from red PDA. The mixture of two different PDA-QD-SiO_2 NPs, bluePDA-QD-SiO_2 NPs not emitting the fluorescence of PDA and redPDA-QD-SiO_2 NPs on which stress was brought on to turn on the PDA fluorescence, was effectively imaged and readily distinguished via fluorescence microscopy, showing their potential for label-free and multiplexed detection of target molecules.

In chapter 3, QDs-embedded silica NPs with an Fe_3O_4 NP core (M-QD-SiO_2 NPs) that has dual functionalities were described. The M-QD-SiO_2 NPs were mono-dispersed in size and exhibited super-paramagnetic and highly fluorescent properties. Most of the M-QD-SiO_2 NPs were naturally internalized into MDA-MB-231 human breast cancer cells, and the NPs containing cells were successfully sorted by utilizing both

fluorescence flow cytometry and a magnetic field. The results indicate that the M-QD-SiO_2 NPs have great potential for multimodal cell separation.

In chapter 4, double-layered Fe_3O_4 NPs containing silica nanoparticles (DL M-SiO_2 NPs) were fabricated with a silica core and highly packed Fe_3O_4 NPs layers. The DL M-SiO_2 NPs had a superparamagnetic property and efficient accumulation kinetics under an external magnetic field. Moreover, the magnetic field-exposed DL M-SiO_2 NPs show quantitative accumulation, whereas single-layered Fe_3O_4 NPs containing silica nanoparticles (SL M-SiO_2 NPs) and silica-coated Fe_3O_4 NPs produced a saturated plateau before full recovery of the NPs. DL M-SiO_2 NPs are promising nanomaterials with a great potential to separate and analyze biomolecules.

Keywords: Multifunctional nanoparticles, Quantum dot, Silica nanoparticle, Superparamagnetic iron oxide nanoparticle, Multiplexed detection

Student number: 2010-20974

TABLE OF CONTENTS

LIST OF TABLES

LIST OF FIGURES

LIST OF ABBREVIATIONS

APTS	(3-Aminopropyl)trimethoxysilane
BALB/c	Bagg Albino (inbred research mouse strain)
CCK-8	Cell counting kit-8
CD44	Cell surface glycoprotein
CdO	Cadmium oxide
CdS	Cadmium sulfide
CdSe	Cadmium selenide
$CHCl_3$	Chlroform
DAPI	4',6-diamidino-2-phenylindole
DCM	Dichloromethane
DIC	N,N'-diisopropylcarbodiimide
DIEA	N,N'-diisopropylethylamine
DL M-SiO_2 NPs	Iron oxide nanoparticles double-layered silica nanoparticles
DLS	Dynamic light scattering
DMF	Dimethylformamide
DNA	Deoxyribonucleic acid
EtOH	Ethyl alcohol
FACS	Flurescence-activated cell sorting
FBS	Fetal bovine serum
FITC	Flurescein isothiocyanate
FRET	Förster resonance energy transfer
FWHM	Full-width-at-half-maximum
HBTU	2-(1H-Benzotriazole-1-yl)-1,1,3,3-tetramethyluronium hexafluorophosphate
HOBt	Hydroxybenzotriazole
HR-TEM	High resolution transmission electron microscopy
HUVEC	Human umbilical vascular endothelial cell
IPA	Isopropyl alcohol
IR	Infra-red

IRM	Image restoration microscopy
LED	Light-emititng-diode
MDA-MB-231	Human mammary gland adenocarcinoma cell line
MPTS	(3-mercaptopropyl)trimethoxysilane
M-QD-SiO_2 NPs	QDs-embedded silica nanoparticles, whose core has an iron oxide nanoparticle
MRI	Magnetic resonance imaging
MTT	3-(4,5-Dimethylthiazol-2-yl)-2,5-diphenyltetrazolium bromide
NIH 3T3	Mouse embryonic fibroblast cell line
NP	Nanoparticle
OA	Oleic acid
ODE	1-Octadecene
PBS	Phosphate buffered saline
PC-3	Human caucasian prostate adenocarcinoma cell line
PCDA	10,12-Pentacosadiynoic acid
PDA	Polydiacetylene
PDA-QD-SiO_2 NPs	Quantum dot-assembled silica nanoparticles bearing a polydiacetylene supramolecule on their surface
PE	Phycoerythrin
PL	Photoluminescence
PVP	Polyvinylpyrrolidone
QD	Quantum dot
QD-SiO_2 NPs	QDs-embedded silica nanoparticles
QY	Quantum yield
RD	Rhodamine
Se	Selenium
SL M-SiO_2 NPs	Iron oxide nanoparticles single-layered silica nanoparticles
SPION	Superparamagnetic iron oxide nanoparticle
TCSPC	Time-correlate single photon counting
TEM	Transmission electron microscopy
TEOS	Tetraethyl orthosilicate

TOP	Triooctylphosphine
TR	Texas red
U-87 MG	Human glioblastoma astrocytoma cell line
UV	Ultra-violet
YFP	Yellow fluorescent protein
$Zn(DMSC)_2$	Zinc dimethyldithiocarbamate
ZnS	Zinc sulfide

Multifunctional and Biocompatible Nanomaterials Based on Multiple Quantum Dots/Iron Oxide Nanoparticles-Embedded Silica Nanosphere

Introduction

1. Quantum Dots (QDs) for Bioapplications

1.1. General Conception of QDs

Quantum dot (QD) is a semiconductor nanocrystal which is small enough to exhibit quantum confinement effect.[1-3] Specifically, when the radius of a semiconductor particle is smaller than its exciton Bohr radius, typically under 10 nm, the energy spectrum of particle becomes discrete. This phenomenon makes the bandgap dependent on size as shown in Fig. 1. Since the bandgap of semiconductor determines the emission range of light, the color of emitted light also becomes subject to the particle size. For example, as the diameter of cadmium selenide (CdSe) nanoparticle increases, the emission spectrum tends to redshift, as shown in Fig. 2.[4,5] Hence, the emission colors of QDs can be tuned by controlling the particle size. Since various semiconductors which have different bandgap alignment could be chosen as the base material of QDs (Fig. 3),[6] QDs can be fabricated to emit broad spectral range from ultra-violet (UV) to near infra-red (IR) wavelength by selecting their base material and size.[7-11]

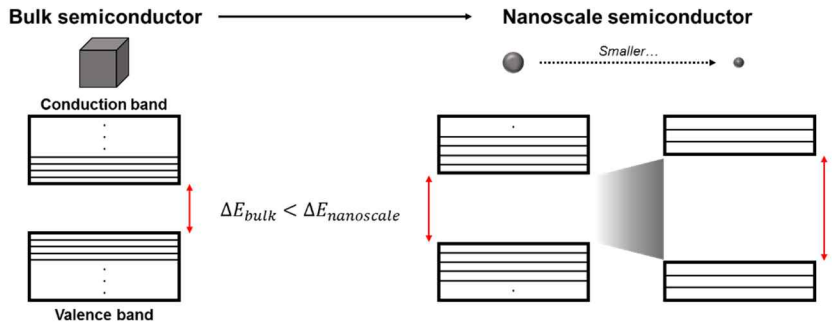

Figure 1. Schematic illustration of the quantum confinement effect.

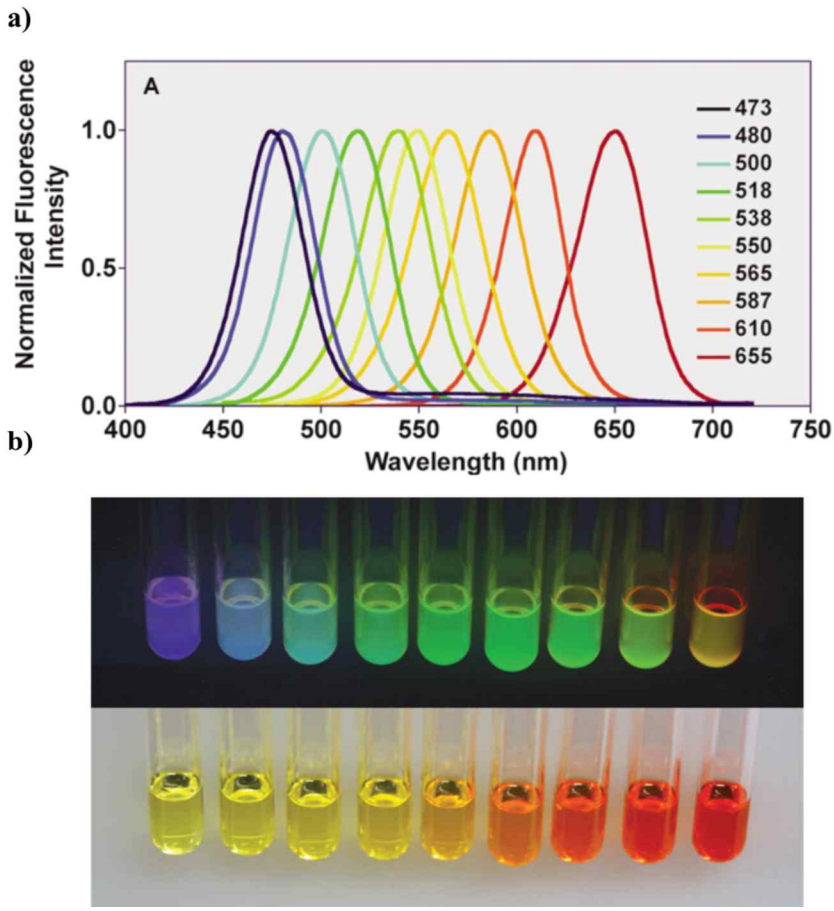

Figure 2. a) Size-tunable fluorescence spectra of CdSe quantum dots (QDs)[4] and b) colloidal suspensions of CdSe QDs of increasing size from left to right under ambient light (bottom) and ultraviolet (top), respectively.[5]

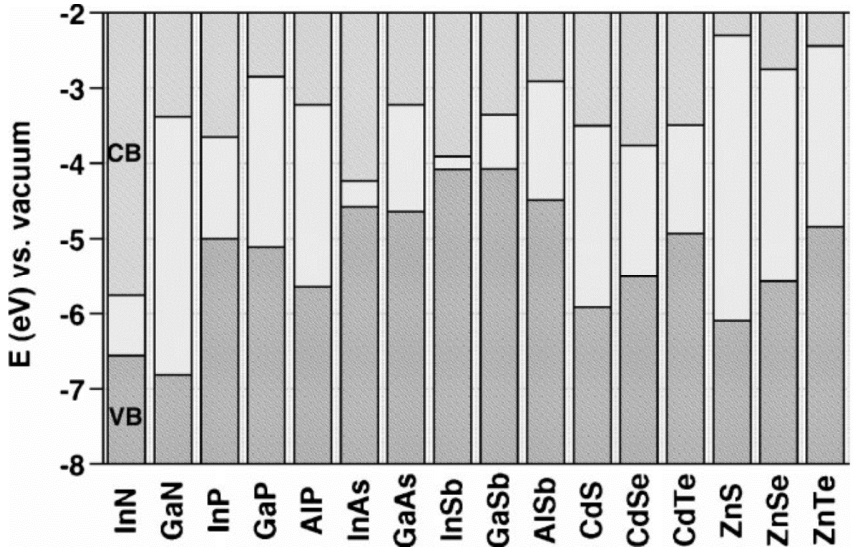

Figure 3. Electronic energy levels of semi-conductors using the valence-band offsets. (VB: valence band, CB: conduction band)[6]

Compared to the organic-based fluorescent dyes, QDs could provide several advantages. First, QDs have a highly narrow emission spectrum, which is ideal for applications of simultaneous detection of multiple fluorescence.[12] Commericialized QDs show narrow and symmetric emission peaks, typically 25-35 nm of full-width-at-half-maximum (FWHM), as shown in Fig. 4.[4] Second, QDs have broad absorption spectra. As well as the emission spectrum of QDs, the absorption spectrum is dependent on the particle size because of quantum confinement effect. Any light source which is shorter than the emission wavelength can excite QDs (Fig. 5).[13] These narrow emission/broad absorption spectrum profiles make possible to emit all fluorescent colors of various QDs simultaneously with a single excitation light source. In addition, QDs have better resistance to photobleaching,[14] larger molar extinction coefficients,[15] higher quantum yields,[16] and longer fluorescence lifetimes compared to organic fluorescent dyes.[17]

For these reasons, QDs have been highlighted as alternative materials of organic dyes in many fields such as photovoltaic devices,[18-24] light-emitting-diode (LED),[25-31] transistors,[32-34] and

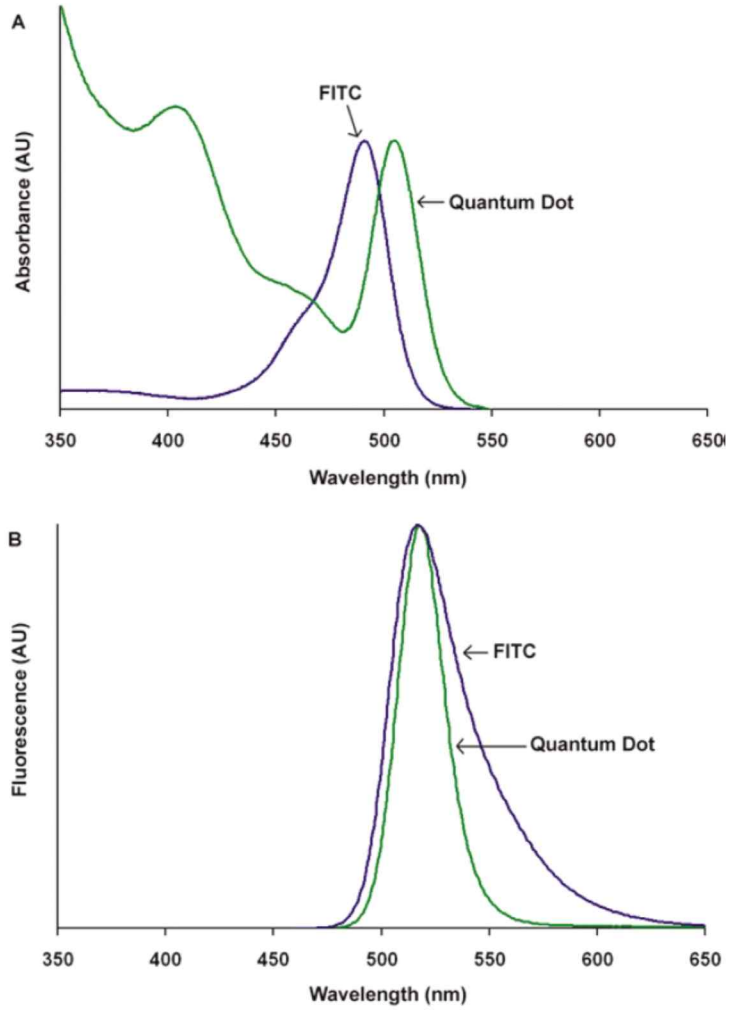

Figure 4. Comparison of (A) optical absorption and (B) fluorescence emission spectra of QDs and organic dyes. The data shown above are for CdSe QDs and fluorescein isothiocyanate (FITC). The emission peaks have nearly identical wavelengths but the QD peak is narrower and more symmetric (~25 nm FWHM).[4]

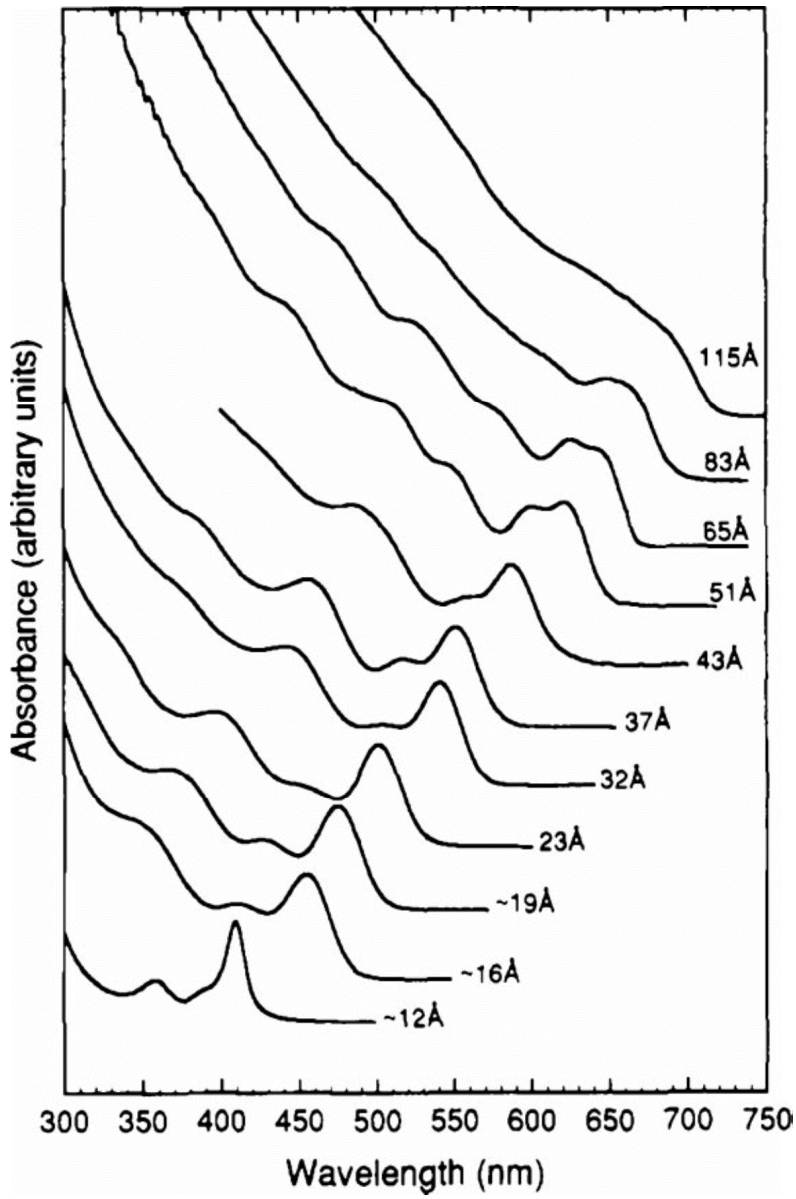

Figure 5. Optical absorption spectra of CdSe nanocrystallites dispersed in hexane, ranging in size from 12 Å to 115 Å.[13]

bioassay.[16,35-42] Especially, as an optical label for various bioassay, QDs have quickly replaced the role of traditional organic dyes for the last decades, due to their superior brightness and stability.[43]

Since fabricated QDs are generally stored at hydrophobic solvent with long alkyl chain ligands,[13,44] direct use of QDs in bioapplication without any surface modification is inappropriate.[42] Hence, the protection of QDs surface by hydrophilic materials should be preceded before the practical bioapplications. However, the surface modification of QDs without careful consideration could lead to a drastical decrease of photoluminescence.[45] The surface modification methods of QDs for aqueous condition have been reported for decades, including surface passivation method[17,35,43,46-51] and ligand exchange method,[52-55] as shown in Fig. 6.

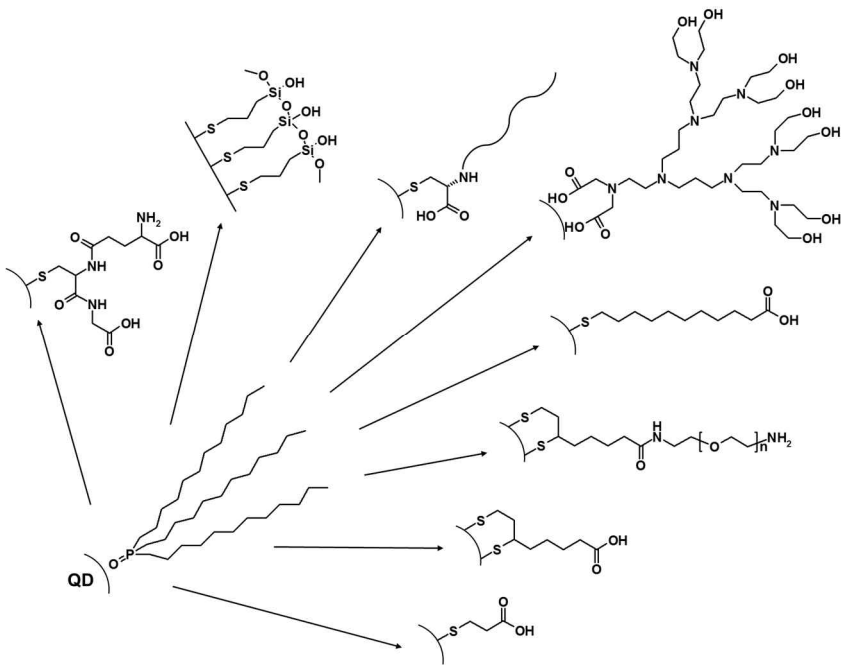

Figure 6. Schematic illustration of various surface modification methods of QDs.[42]

1.2. Silica Encapsulated QDs

Silica encapsulation is an useful method to protect fluorescence property of QDs in an aqueous condition. Silica encapsulation could provide many advantages, such as water compatibility, facile chemical modification, low cytotoxocity, and excellent chemical inertness.[56,57] Thus far, various studies for silica encapsulation of single QDs have been published.[46,58-61]

Nanoprobes containing multiple QDs have also been developed for better optical characteristics.[62-66] When silica NPs are used as a template for embedding multiple QDs, they can provide additional advantages, such as easier control of size affording multifunctional properties. Multiple QDs-incorporated silica nanostructure can be brighter than single QDs due to their greater number on it. However, significant decrease in the QY of the employed QDs could be encountered during the silica encapsulation process.[67,68]

2. Superparamagnetic Iron Oxide Nanoparticles for Bioapplications

2.1. General Conception of Superparamagnetic Nanoparticles (NPs)

Magnetic nanoparticles (MNPs) of 10-20 nm sizes are known to have a single magnetic domain, maintaining one large magnetic moment under the blocking temperature (T_b). When the temperature is above the T_b, thermal energy induces free rotation of magnetic NPs, causing loss of the net magnetization in the absence of an external magnetic field (Fig. 10a). This superparamagnetic behavior exhibits negligible remnant magnetization after the removal of external fields and enables the particles to avoid agglomeration at room temperature,[69-74] as shown in Fig. 10b. Due to this unique property, MNPs are of great interest in various biotechnology fields, particularly in the field of biomolecule separation.[75-77] MNPs have been synthesized with various base materials; iron oxides,[78-80] pure metals,[81,82] spinel-type ferromagnets,[83,84] and alloys.[85,86] Among various MNPs,

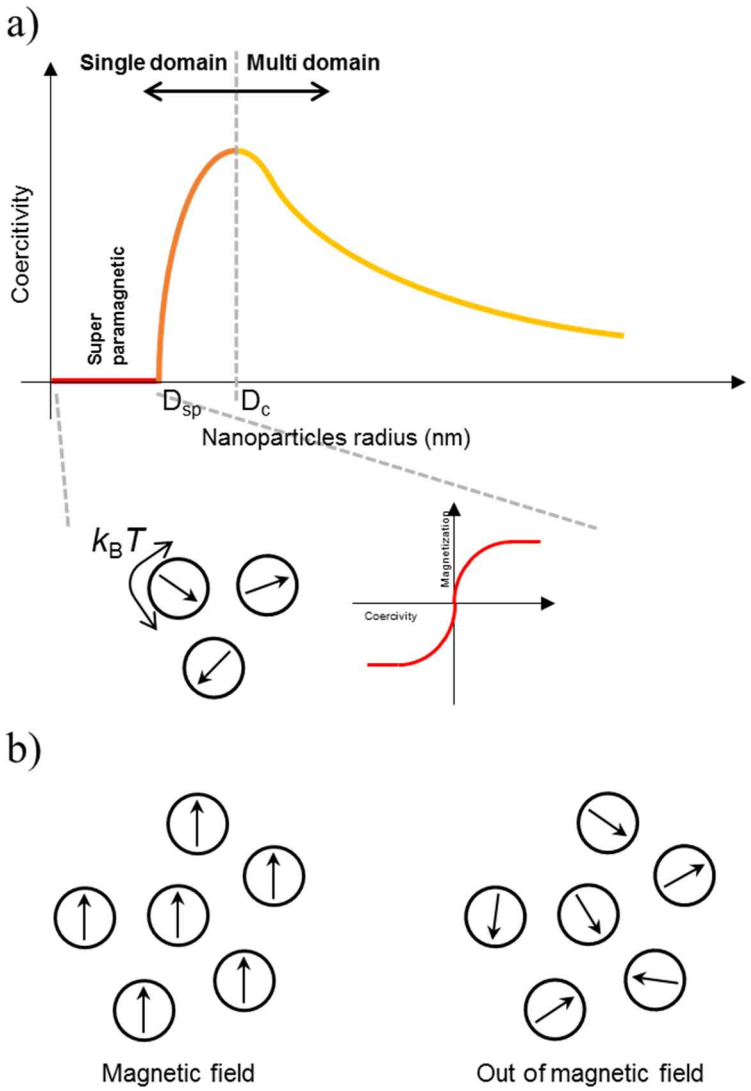

Figure 7. Schematic illustration of the superparamagnetism. (a) Coercivity-size relations of small magnetic particles; D_{sp} = superparamagnetic diameter, D_c = single domain critical diameter, and (b) magnetization behavior of superparamagnetic nanoparticles.

Fe_3O_4 NPs are promising because they are nontoxic, and the synthetic methods have been relatively well-established.[69]

However, bare Fe_3O_4 NPs are hampered by several drawbacks for use in biomolecule separation. For example, a single Fe_3O_4 NP itself shows very slow accumulation behavior and low separation yield by magnet. Moreover, Fe_3O_4 NPs are highly vulnerable to oxidative condition, which would damage the magnetism and dispersion property of NPs.[87,88]

2.2 Magnetic Nanoparticles (NPs) on Silica

Silica has been widely incorporated in various NPs, because it is nontoxic, biocompatible, optically transparent, chemically inert, and has a well-known surface chemistry. Silica encapsulation method could also overcome several agglomeration factors; incomplete coordination of surface atoms of NPs,[69,89,90] and van der Waals interaction.[91,92] Thus, a lot of magnetic-silica composite materials have been reported.[63,93,94] Among them, multiple magnetic NPs incorporated silica NPs could have merits such as quicker accumulation kinetics under an external magnetic field than a single Fe_3O_4 NP while maintaining their superparamagnetic property. They can be divided into two categories; Fe_3O_4 NPs could be “incorporated” into the inner space of silica structure, or “immobilized” onto the surface of silica backbone, as shown in Table 1.[95] In case of Fe_3O_4 NPs “incorporated” silica NPs, the size control of NPs and limited fabrication scale could be a problem. Thus, Fe_3O_4 NPs “immobilized” silica NPs could solve those problems.

Table 1. Previous Works of Magnetic NPs-assembled SiO_2 Nanostructures

Type	Structure	Size	Applications
Single MNP with silica shell[96-99]	 Fe_3O_4@SiO_2	Normally <100 nm	Cell sorting and imaging, MRI etc.
Multiple MNPs "incorporated" into the inner space of a silica structure[100-102]	 Multi number of Fe_3O_4 core@SiO_2	Normally <micro	Cell sorting and imaging, MRI etc.
	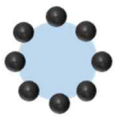 SiO_2@Fe_3O_4	Submicro	MRI and cell sorting
Multiple MNPs "immobilized" onto the surface of silica backbone[93,103-106]	 Hollow SiO_2@MNP+shell	Submicro	Cell uptake and drug delivery
	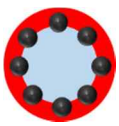 SiO_2@Fe_3O_4+ Au NPs@Au shell	Submicro	DNA-probe

* : SiO_2, ●: Fe_3O_4 NPs, : Au

3. Research Objectives

In this thesis, quantum dots and/or superparamagnetic iron oxide NPs assembled multifunctional nanospheres for bioapplication are described. We used silica as a support matrix of the designed NP structure, because silica can provide many advantages, such as water compatibility, facile chemical modification, low cytotoxicity, and excellent chemical stability.

In chapter 1, highly bright QDs-embedded silica NPs (QD-SiO_2 NPs) for bio-imaging are described. We developed a method for embedding QDs onto a carrier template so that a large number of hydrophobic QDs can be attached to hydrophilic silica NP. We have also demonstrated the key advantages of QD-SiO_2 NPs compared with single QD in terms of brightness, toxicity, and in vitro analysis.

In chapter 2, QD-assembled silica NPs bearing a polydiacetylene supramolecule on their surface (PDA-QD-SiO_2 NPs) as a label-free sensing platform towards multiplexed optical detection of biological molecules are described. QDs on PDA-QD-

SiO_2 NPs play a role as an encoder to designate the kind of target, and the PDA on their surface is utilized as a signal transducer to report target recognition via its chromic change properties. To demonstrate their potential use for label-free and multiplexed detection, we show that a mixture of two kinds of PDA-QD-SiO_2 NPs, bluePDA-QD-SiO_2 NPs and redPDA-QD-SiO_2 NPs, can be effectively imaged and that the redPDA-QD-SiO_2 NPs emitting the fluorescence from the red-PDA is readily distinguished from nonfluorescent bluePDA-QD-SiO_2 NPs via fluorescence microscopy.

In chapter 3, we describe the preparation of QDs-embedded silica NPs, whose core has an iron oxide NP (M-QD-SiO_2 NPs). These multifunctional NPs are uniform in size and super-paramagnetic with intense fluorescence. M-QD-SiO_2 NPs were characterized using two kinds of cell separation methods: fluorescence-activated cell sorting (FACS) and magnetic field induced cell separation. These assessments are performed to determine the potential of M-QD-SiO_2 NPs as a tool for biomedical applications, particularly multimodal bioseparation.

In chapte 4, double-layered Fe_3O_4 NPs embedded silica nanoparticles (DL M-SiO_2 NPs) with a core/multi-shell structure are described. The catecholate-iron complexation method was utilized to increase the loading level of Fe_3O_4 NPs on the silica NPs. The DL M-SiO_2 NPs which contain a large number of Fe_3O_4 NPs on the surface of a silica NP core (~200 nm) have monodispersity with fast response for an external magnetic field with superparamagnetic property. The exploited Fe_3O_4 NPs were well protected by silica shell from the aforementioned weakness. Finally, the capability of DL M-SiO_2 NPs to separate proteins was demonstrated using ligand-conjugated DL M-SiO_2 NPs

Chapter I.
Fabrication of Quantum Dot-Assembled Silica Nanoparticles

1. Experimental Section

1.1. Chemicals and Materials

All chemicals were used as received without further purification. Cadmium oxide (CdO), selenium (Se), trioctylphosphine (TOP), oleic acid (OA), 1-octadecene (ODE), octanethiol, zinc dimethyldithiocarbamate ($Zn(DMSC)_2$), sulfur, tetraethyl orthosilicate (TEOS), (3-mercaptopropyl)trimethoxylsilane (MPTS), tetramethylammonium hydroxide (TMAH) and 3-mercaptopropionic acid (MPA) were purchased from Sigma Aldrich (St. Louis, MO, USA). Chlroform ($CHCl_3$), dichloromethane (DCM), ammonia aqueous solution (27%) and ethanol (EtOH) were purchased from Daejung Chemicals (Gyeonggi-do, South Korea).

1.2. Preparation of Quantum Dot-Assembled Silica Nanoparticles (QD-SiO_2 NPs)

Preparation of QDs

CdO (0.1284 g) and $Zn(DMSC)_2$ (1.520 g) were dissolved in OA (1.695 g) and ODE (20 mL) under N_2 atmosphere, and heated to 100°C under vacuum for 1 h. The solution was further heated to 320°C to form a transparent solution and injected into a precursor solution, which was prepared by dissolving Se (0.078 g) in TOP (1 mL). The growth temperature was set to 300°C for 5 min and then the solution was cooled to room temperature. The final QDs were dispersed in $CHCl_3$ to obtain a 50 mg/mL solution.

Preparation of SiO_2 NPs

First, TEOS (1.6 mL) and ammonia aqueous solution (27%, 3 mL) were added to EtOH (35 mL) containing water (5 mL), followed by vigorous stirring for 20 h at 25°C. The resulting SiO_2 NPs (120 nm) were washed and then dispersed in EtOH.

QDs Conjugation onto the Surface of SiO_2 NPs

Thiol functionalization of the SiO_2 NPs (4 mL, 50 mg/mL suspension in EtOH) was accomplished by mixing with MPTS (40 uL) and ammonia aqueous solution (40 μL), followed by stirring for 12 h at 25°C. These thiol-modified SiO_2 NPs were washed several times with EtOH and then dispersed in EtOH. The QDs (3.5 mL, as-prepared above) and thiol-modified SiO_2 NPs (2 mL, 50 mg/mL in EtOH) were injected into a vial in series and then stirred vigorously for a few seconds. Then, MPTS (55 uL) and ammonia aqueous solution (55 uL) were introduced to the QD-SiO_2 NPs mixture, and shaken by shaking for 1 h at 25°C. The resulting mixtures were washed with EtOH several times and dispersed in EtOH (20 mL) containing TEOS (0.2 mL) and ammonia aqueous solution (0.2 mL). After shaking for 12 h, the QD-SiO_2 NPs were centrifuged and washed with EtOH several times.

1.3. Preparation of Water Soluble Single QD

Purified QDs s were dispersed in $CHCl_3$ to obtain a 0.1 μM QDs solution. TMAH (100 mg) was mixed well with MPA in 1 mL of $CHCl_3$. The amount of MPA was varied between 5 to 100 μL to determine its effect on the ligand-exchange reaction. After 15 min of mixing, a clear colorless aqueous layer (about 10% of total volume) was formed above the $CHCl_3$ layer. The biphasic solution was mixed by vigorous shaking and allowed to stand for 1 h in order to equilibrate. The lower organic phase, which contained deprotonated MPA, was transferred into a vial for ligand-exchange reaction with QDs or mQDs. One hundred microliters of TOP-capped QDs (0.1 μM in $CHCl_3$) was added to the MPA-$CHCl_3$ solution and mixed well. The solution was allowed to stand at room temperature for 1–5 h. After the reaction, the MPA-capped QDs that had been separated from the $CHCl_3$ solutions were collected, washed with $CHCl_3$ for twice, and dispersed in 1.0 mL of water.

1.4. Analysis of NPs

Optical Characterization

UV-vis absorption spectra were recorded with a UV-spectrometer. Photoluminescence (PL) spectra were recorded using a 6500 Photoluminescence spectrometer (JASCO).

Optical UV Stability

QDs samples were exposed to a UV irradiation source to monitor the UV stability. The distance between samples and the UV lamp was 10 cm. The variation in wavelength shift was less than 5% after exposure to UV for 3000 h.

1.5. *In vitro* Analysis of QD-SiO_2 NPs

In vitro Luminescence Signal Detection

QD-SiO_2 NPs (1.1×10^{12} / mL, stock concentration: 5 mg/ mL) suspended in absolute EtOH was centrifuged at 6,500 rpm for 1 min and phosphate buffered saline (PBS) solution was added. QD-SiO_2 NPs or single QDs (100 μg/20 μl) in PBS solution was added to a Dark 96 well microplate, and the fluorescence signal was detected using an Infinite M200 Fluorometer (Tecan, GmbH, SZ, Austria) at an optimized excitation/emission wavelength of 400/610 nm. Fluorescence signal intensities of each single QDs- or QD-SiO_2 NPs- containing well plate were normalized to those of PBS-containing well plate.

Cytotoxicity Studies

HeLa cells, human cervical carcinoma, which was maintained in DMEM medium (Gibco, Grand Island, NY) containing fetal

bovine serum (FBS, Invitrogen, Grand Island, NY), 10 U/mL penicillin (Invitrogen, Grand Island, NY), and 10 μg/mL streptomycin were inoculated in a 96-well microplate, and single QDs or QD-SiO_2 NPs of increasing concentration ranging from 10 to 40 μg were transferred to the seeded HeLa cells. After incubation for 24 h at 37°C, the cellular toxicity was examined using a simple cellular toxicity kit, CCK-8 (cell counting kit-8, Dojindo Molecular Tech, Inc, Rockville). The incubated cell medium was clearly removed via a PBS washing step, and 10 μl of the CCK-8 solution containing fresh cell medium was placed into each 96-well microplate. After incubation of the CCK-8–treated samples for 2 h, their absorbance at 450 nm was recorded using a microplate reader.

Confocal Laser Microscope Analysis

HeLa cells (2×10^5) were seeded on clean coverslips in a 6-well plate, followed by incubation for 24 h at 37°C. The cells were rinsed using PBS, and single QDs or QD-SiO_2 NPs were then

treated to the cells, and incubated for 24 h. single QD- or QD-SiO_2 NPs-treated HeLa cells were fixed using 4% paraformaldehyde solution (Wako, Pure Chem., Osaka, Japan) under mild shaking conditions for 20 min. Cells were vigorously washed three times using PBS, and attached onto the coverslip using a mounting solution containing DAPI solution (Vector Laboratories, Inc, CA). Confocal microscope images were analyzed using Zeiss LSM image examiner. For DAPI imaging, HFT 405/488 nm light was used as excitation source and the emission wavelength was filtered in wavelength range of 420-480 nm. For QDs imaging, HFT 405/488/543/633 nm light was used as excitation source and the emission wavelength was filtered in wavelength range of 604-754 nm.

2. Results and Discussion

2.1. Design of QD-SiO_2 NPs

The fabrication flow of the proposed highly bright QD-SiO_2 NPs is illustrated in Fig. 8. The diameter of the silica core NPs is approximately 120 nm. QDs were embedded on the surface of silica NPs, a carrier template, for easy handling and size control, and reproducible preparation of nanomaterials. Then, they were encapsulated by a silica shell for providing biocompatibility and easy functionalization.

The photoluminescence maxima of QDs vary from 450 to 650 nm depending on the precursor ratio (Fig. 9a and b). They exhibit high fluorescence quantum yields reaching up to 80%. They display monodispersity of *ca* 6 nm diameter by controlling the shell thickness in large scale synthesis (Fig. 9c and d).

To fabricate QD-SiO_2 NPs, 120-nm SiO_2 NPs were prepared by the Stöber method and used as a carrier template for QDs (Fig. 10a and b).

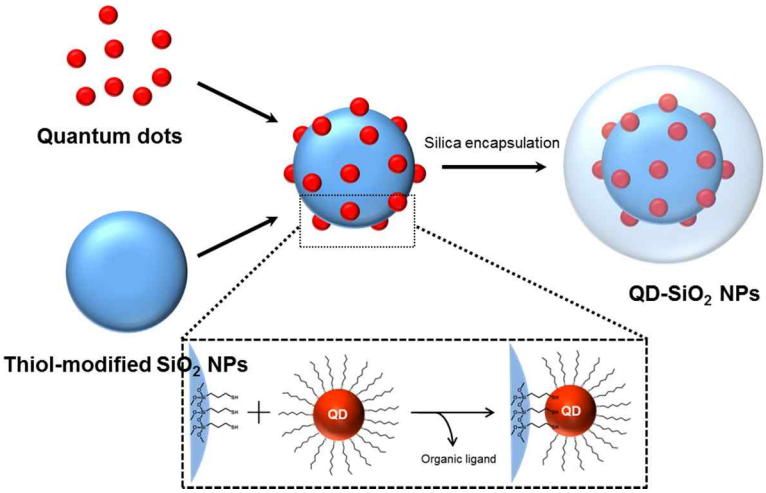

Figure 8. Illustration of synthesis of Quantum dot-assembled silica nanoparticles (QD-SiO_2 NPs). Core-shell CdSe@CdS@ZnS QDs were immobilized to thiol-modified SiO_2 NPs. Then, QD-SiO_2 NPs were prepared by silica shell encapsulation.

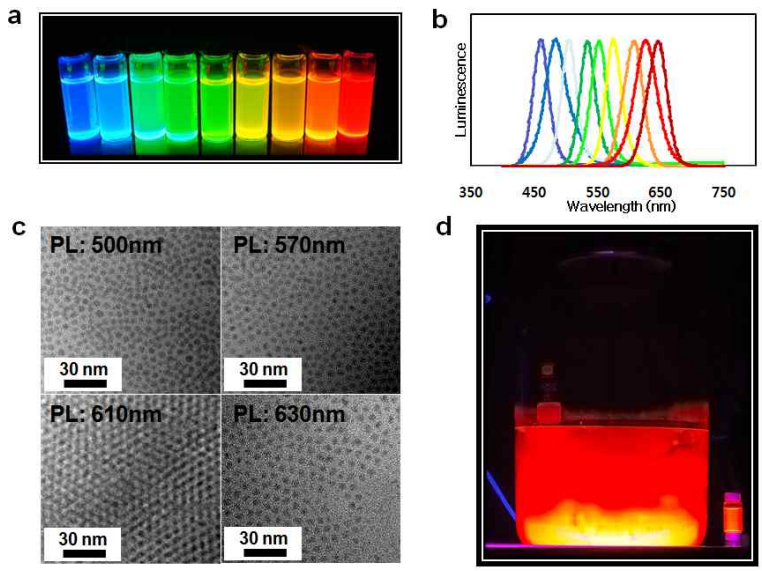

Figure 9. Characterization of QDs; (a) photograph of various QDs, (b) photoluminescence spectra of QDs, (c) TEM images of various QDs, (d) photograph of sub kilogram amount of QDs.[107]

The embedding of a large number of hydrophobic QDs to cover the entire surface of a hydrophilic silica backbone was a challenging process. The silica NPs were functionalized with a thiol group using MPTS as an organosilane coupling agent because it has high affinity to QDs. However hydrophilic properties were exhibited in the thiol-functionalized silica NPs in contrast to QDs, which have a TOP layer and possessed hydrophobic properties. We controlled the ratio and the amounts of hydrophilic and hydrophobic solvent for efficient mixing of silica NPs and QDs to embed hydrophobic QDs onto hydrophilic thiol-modified silica NPs. If an amphiphilic polymer is used,[108] it can cause reduction of QY upon further silica shell coating. The QDs-embedded silica NPs were collected for analysis by centrifugation. HR (High resolution)-TEM analysis revealed that the QDs-embedded silica NPs had rough surfaces most likely due to the embedding of QDs on the surface of the silica core (Fig. 10c). A lattice structure of the QDs was observed on the surface of the silica NPs, as shown in Fig. 10d. The number of QDs on the silica core was estimated to be 200~300 per single SiO_2 NP.

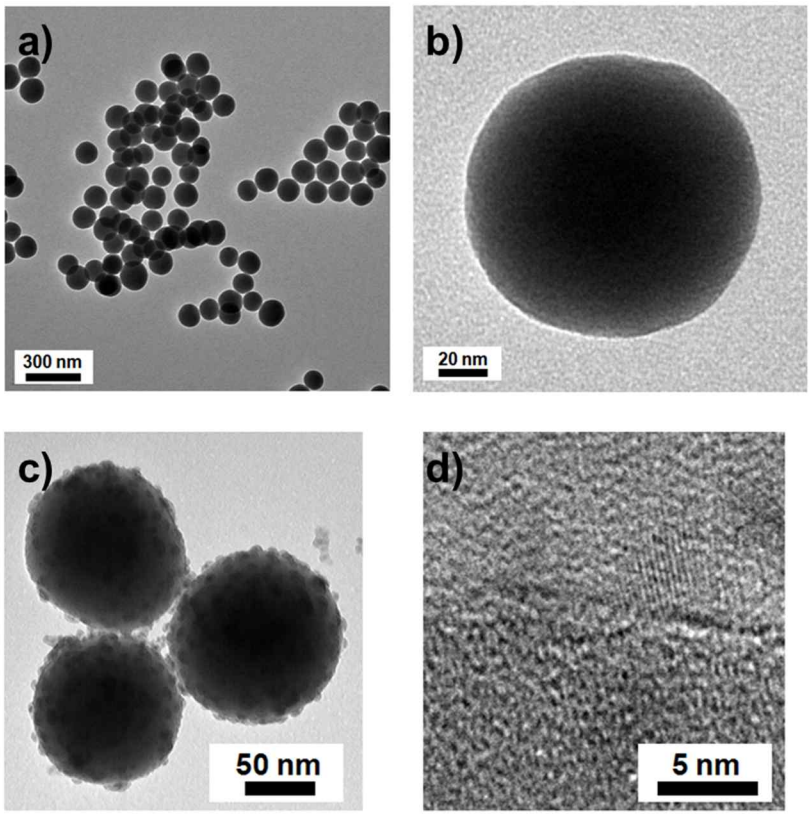

Figure 10. TEM images of (a, b) 120-nm silica NPs and (c) QD-embedded SiO_2 NPs. HR-TEM images of (d) QD-embedded SiO_2 NPs.[107]

The MPTS-treated QDs-embedded silica NPs were dispersed in EtOH. They were subsquently encapsulated by a silica shell with TEOS. As shown in Fig. 11a, *ca.* 300 QDs were embedded on a silica NP, and a thin silica layer was formed around the QDs-embedded silica NPs. The QD density on the silica surface was calculated as *ca.* 0.7 unit per 100 nm^2. The QD-SiO_2 did not coagulate during the silica coating step and was well dispersed in water, possessing characteristic PL properties (Fig. 11c).

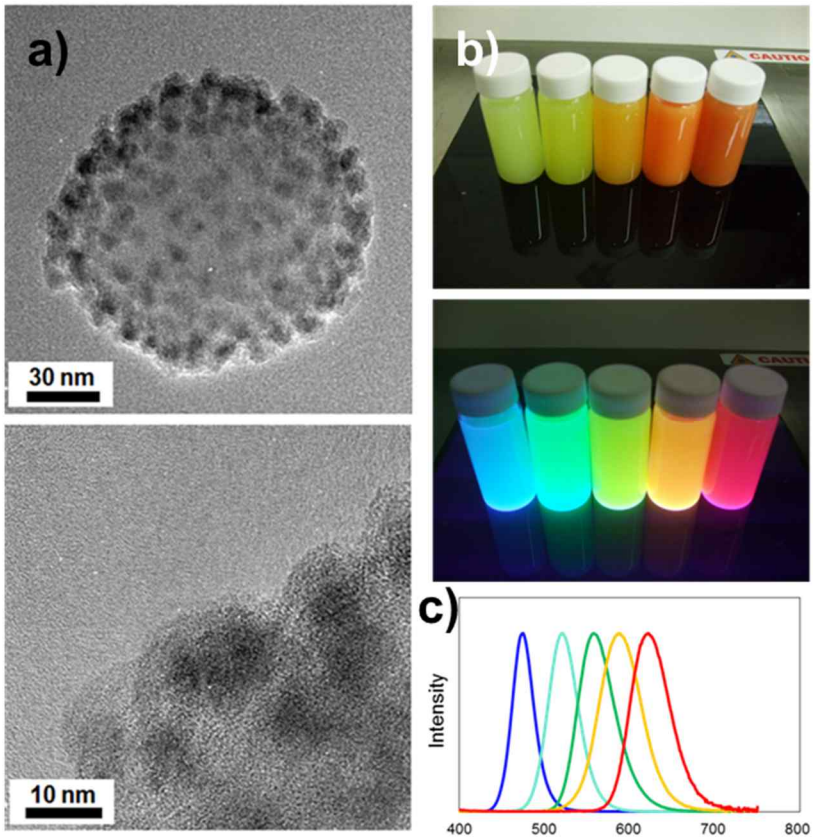

Figure 11. Characterization of QD-SiO_2 NPs. a) TEM images of QD-SiO_2 NPs. b) Photographs of various QD-SiO_2 NPs from QDs with emission maximum at 470, 520, 550, 580, and 615 nm under daylight and UV light, respectively. c) The PL emission of the corresponding QD-SiO_2 NPs.[107]

2.2. Comparison of Single QDs and QD-SiO_2 NPs

To compare the fluorescence intensity of QD-SiO_2 NPs, which has approximately 500 unit of single QDs, with that of single QD (sQD), photoluminescence signals from QD-SiO_2 NPs and an equivalent number of sQDs were examined in an 1.5 mL microtube. Photoluminescence images of the tubes revealed significantly amplified luminescence activity of QD-SiO_2 NPs compared to sQDs (Fig. 12a). Quantitative fluorescence analysis using a fluorometer showed *ca* 200-times higher fluorescence intensity from the QD-SiO_2 NP samples than from the sQD samples (Fig. 12b).

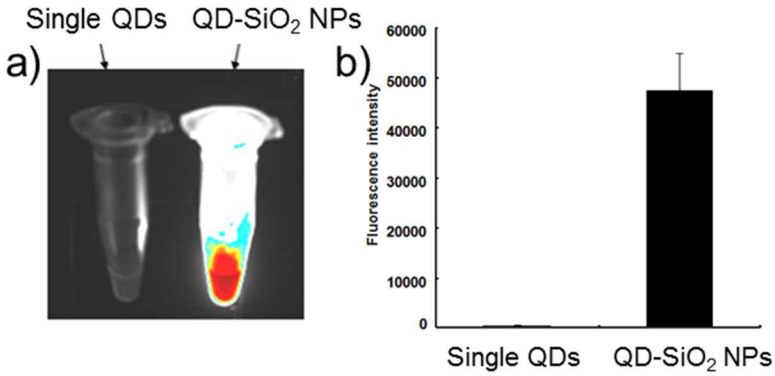

Figure 12. Comparison of fluorescence intensities of single QDs and QD-SiO_2 NPs. a) Fluorescence images of single QD (left) and QD-SiO_2 NPs (right) containing tubes and b) their fluorescence intencities of single QDs (left) and QD-SiO_2 NPs (right).[107]

2.3. *In vitro* Luminescence Signal Aquisition

To confirm whether the natural uptake of QD-SiO_2 NPs occurs in cells, QD-SiO_2 NPs were incubated in HeLa cells for 24 h. Confocal microscopic images confirm that most of the QD-SiO_2 NPs are distributed in the cytoplasmic area of cells (Fig. 13). The transfection efficiency of QD-SiO_2 NPs in cells was analyzed in 24 h after transfection. The fluorescence signals in the supernatant and trypsinized-cell pellets were measured using a fluoremeter. We found that the transfection efficiency in QD-SiO_2 NPs-transfected cell pellets was 88%. Nanomaterials of appropriate size are known to be allowed for intracellular uptake by natural endocytosis. We confirmed that 120-nm-sized QD-SiO_2 NPs could accumulate easily inside cells without cell penetrating peptides such as TAT.

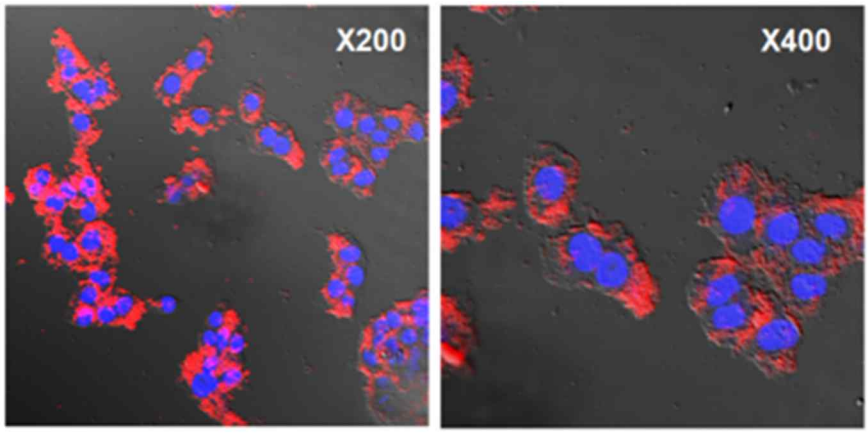

Figure 13. Fluorescence images of QD-SiO_2 NPs-uptaken HeLa cells (Red color: QD, Blue color: DAPI).[107]

2.4. Tracking of Stem Cell Differentiation Using QD-SiO_2 NPs

To confirm whether the QD-SiO_2 NPs could be exploited to track stem cell differentiation, QD-SiO_2 NPs were incubated in HUVECs for 12 h at 37°C. After the incubation, angiogenesis assay was performed to measure the cell differenciation ability of the NPs-uptaken HUVECs. After 12 hr, the tube formation of endothelial cells was confirmed by both fluorescence of cell internalized QD-SiO_2 NPs and F-actin, indicating that the new blood vessels were successfully differenciated from the NPs-uptaken HUVECs, as shown in Fig. 14. This results show that the QD-SiO_2 NPs neither inhibit the angiogenesis process of HUVECs nor lose their fluorescence intensity during the cell differenciation.

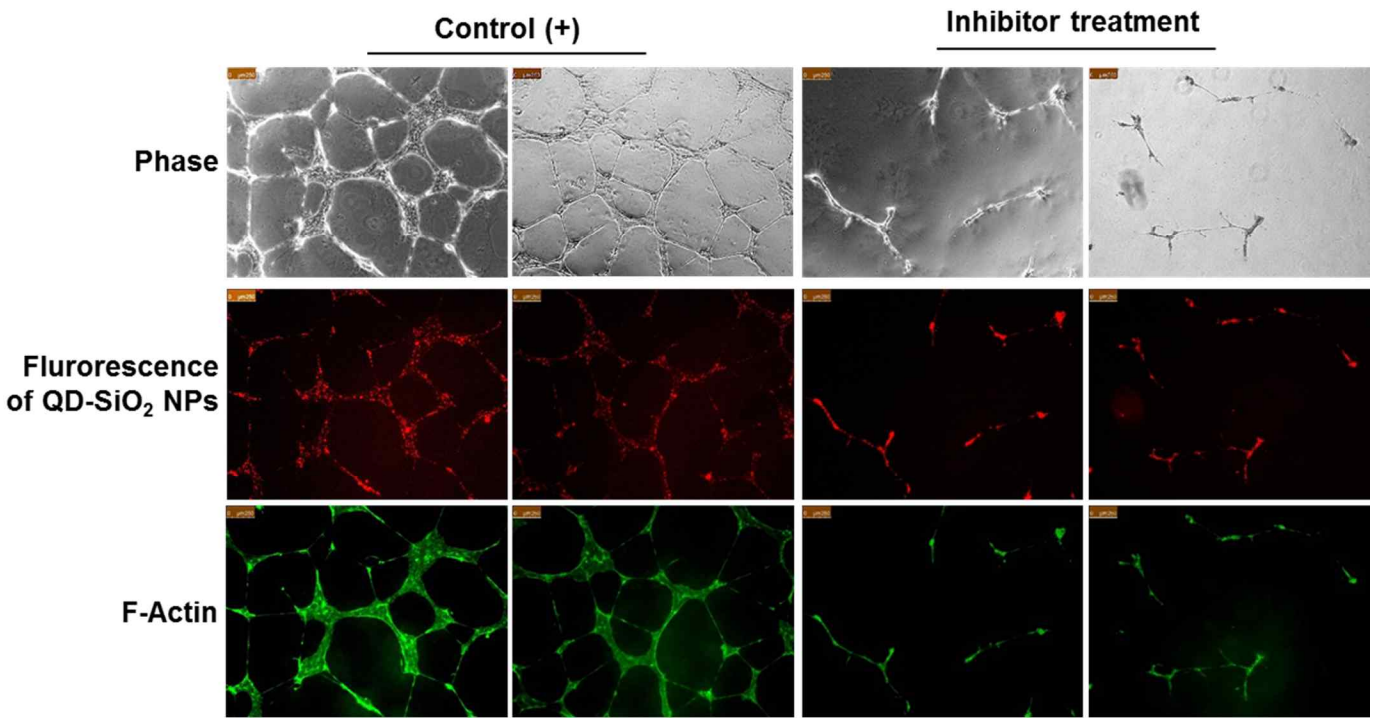

Figure 14. Angiogenesis assay using human umbilical vein endothelial cells (HUVECs), incubated with QD-SiO_2 NPs.

Chapter II.
Fabrication of Quantum Dot-Assembled Silica Nanoparticles with Polydiacetylene Supramolecule

1. Experimental Section

1.1. Chemicals and Materials

All chemicals were used as received without further purification. Cadmium oxide (CdO), selenium (Se), trioctylphosphine (TOP), oleic acid (OA), 1-octadecene (ODE), octanethiol, zinc dimethyldithiocarbamate ($Zn(DMSC)_2$), sulfur, tetraethyl orthosilicate (TEOS), (3-mercaptopropyl)trimethoxylsilane (MPTS), (3-aminopropyl)trimethoxysilane (APTS), 10,12-pentacosadiynoic acid (PCDA) and *N,N′*-diisopropylcarbodiimide (DIC) were purchased from Sigma-Aldrich (St. Louis, MO, USA). *N,N′*-Diisopropylethylamine (DIEA) was purchased from Alfa Aeasar (Ward Hill, MA, USA). Chlroform ($CHCl_3$), dichloromethane (DCM), ammonia aqueous solution (27%) and ethanol (EtOH) were purchased from Daejung Chemicals (Gyeonggi-do, South Korea).

1.2. Preparation of Quantum Dot-Assembled Silica Nanoparticles Coated with Polydiacetylene Supramolecule (PDA-QD-SiO_2 NPs)

Immobilization of 10,12-pentacosadiynoic acid (PCDA) on SiO_2 NPs and QD-SiO_2 NPs

The bare SiO_2 NPs and QD-SiO_2 NPs (1 mL, 10 mg/mL in EtOH) were functionalized with amino groups by reacting with APTS (10 μL) and ammonia aqueous solution (10 μL) for 12 h at 25°C. The resulting NPs were centrifuged at 7500 rpm for 5 min and washed with DMF and DCM. The PCDA monomer (80 μmol) was dissolved in DCM (10 mL), and sonicated for 20 min until it was fully dispersed. This PCDA monomer solution was added to the amine-functionalized NPs (1 mL, 10 mg/mL in DCM) with DIC (80 μmol) and DIEA (80 μmol). The reaction mixture was sonicated for 10 min and stirred for 12 h at 25°C. The NPs were washed with DCM, EtOH, and water and dispersed in water.

Photo-Polymerization of PCDA Immobilized SiO_2 NPs and QD-SiO_2 NPs

The PCDA monomer (10 μmol) was dissolved in $CHCl_3$ (10 mL) and sonicated for 20 min until the PCDA monomer was fully dispersed, and then the solvent was evaporated. Then, water (10 mL) was added to the remaining PCDA solid residue, and the resulting solution was sonicated for 20 min and filtered. To fabricate PDA-conjugated NPs, the PCDA immobilized SiO_2 NPs or QD-SiO_2 NPs (1 mL, 10 mg/mL in water) were dispersed in the PCDA monomer solution, and stored for 5 h at 4°C to self-assemble the PCDA completely. Then, the mixture was exposed to UV (254 nm) for 5 min for obtaining PDA-QD-SiO_2 NPs or PDA-SiO_2 NPs. The final NPs were centrifuged and washed with water.

Applying Stress on PDA-QD-SiO_2 NPs

The prepared PDA-QD-SiO_2 NPs were heated at 100°C for 5 min. Then the NPs were cooled to room temperature.

1.3. Analysis of Nanoparticles (NPs)

Physical Property Analysis

Transmission electron microscopy (TEM) analysis was performed on a Libra 120 (Carl Zeiss, Germany) operating at 120 kV. High resolution transmission electron microscopy (HR-TEM) analysis was performed on a JEOL JEM-3010 (JEOL, Japan) operating at 300 kV. All the samples for TEM analysis were deposited on a 300 mesh holey carbon grid. Hydrodynamic size analysis was performed on a ELSZ-1000 dynamic light scattering (DLS) spectroscope (Otsuka, Japan). All the samples for DLS analysis were dispersed in EtOH.

Optical Property Analysis

Fluorescence photographs were obtained under ultra-violet (365 nm) exposure powered by an UV source (Dong Seo Science, Korea). The samples were exposured at a point 15 cm away from

the 4 W lamp. Photoluminescence (PL) spectra were obtained using a FP-6500 fluorescence spectrometer (JASCO, Japan). All the samples for PL analysis were dispersed in EtOH and exposed to a laser source (390 nm).

1.4. Multiplexed Optical Detection of NPs

To demonstrate the potential use for label-free and multiplexed detection on PDA-QD-SiO_2 NPs, we mixed the PDA-QD-SiO_2 NPs and the heat treated PDA-QD-SiO_2 NPs together in a 1:1 ratio in an aqueous solution and measured their fluorescence using a DeltaVision RT image resotration microscope (Applied Precision, USA) equipped with a RD-TR-PE filter (617 nm), a DAPI filter (457 nm), and a YFP filter (535 nm).

2. Results and Discussion

2.1. Preparation of PDA-SiO_2 NPs and PDA-QD-SiO_2 NPs

The preparation method of the PDA-QD-SiO_2 NPs, as a label-free and multiplexed sensing-platform, is illustrated in Fig. 15. QD-embedded silica (QD-SiO_2) NPs were prepared based on the method reported previously.[107] The TEM images of silica NPs used for synthesis of QD-SiO_2 NPs are shown in Fig. 16. QDs with different emission maxima at 490 and 540 nm (blue and green colors) were embedded on the silica NP surface as an encoder for designating the kind of target molecule, and the resulting NPs were encapsulated with a silica shell. As shown in Fig. 17a, the size of QD-SiO_2 NPs was approximately 300 nm, which is larger than half of the illuminating wavelength, indicating that the imaging resolution may not be restricted by the diffraction limit[109]. In addition, the QDs were densely embedded on the silica surface.

Approximately 2,000 QDs were embedded per silica NP. These QD-SiO_2 NPs were not cytotoxic based on MTT assay results.[107]

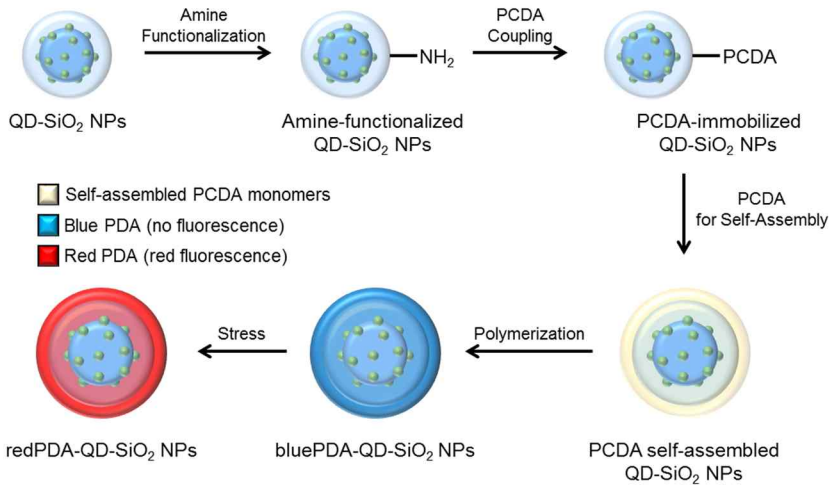

Figure 15. Scheme for the preparation of quantum dot (QD)-assembled silica nanoparticles bearing a polydiacetylene (PDA) supramolecule on their surface (PDA-QD-SiO_2 NPs).[110]

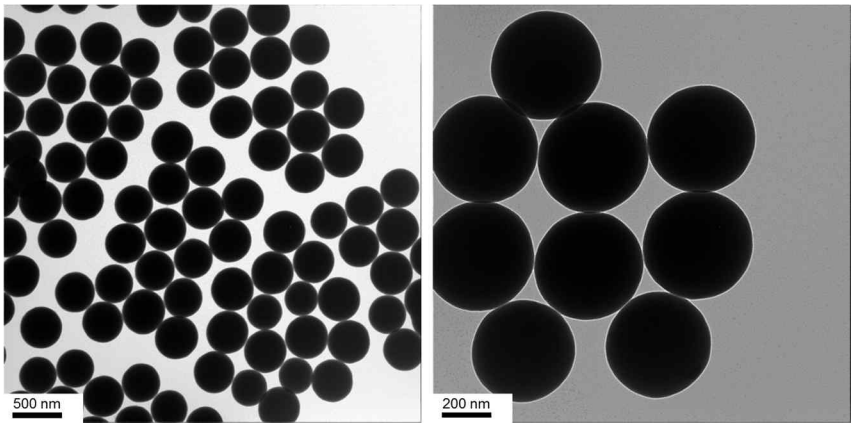

Figure 16. Transmission electron micrograph images of bare silica nanoparticles (NPs).[110]

Next, we introduced amino groups on the surface of QD-SiO_2 NPs with APTS to couple PCDA monomers for photo-polymerization.[111-115] Then, additional PCDA was added to QD-SiO_2 NPs bearing PCDA on their surface, and the resulting mixture was incubated at 4°C for 5 h for the PCDA monomers to self-assemble on QD-SiO_2 NPs surface. As shown in Fig. 17c, the PCDA monomers were stacked as multiple layers on the surface of QD-SiO_2 NPs during incubation. After UV irradiation, polymerization of PCDA was initiated, and a 20 nm layer of PDA was formed on the surface of QD-SiO_2 NPs as shown in Fig. 17b. After polymerization, we measured the hydrodynamic size of QD-SiO_2 NPs coated with PDA (PDA-QD-SiO_2 NPs) using dynamic light scattering (DLS). As shown in Fig. 18, the hydrodynamic size of PDA-QD-SiO_2 NPs was 600-900 nm, and the NPs contained a small portion of nanoparticle aggregates.

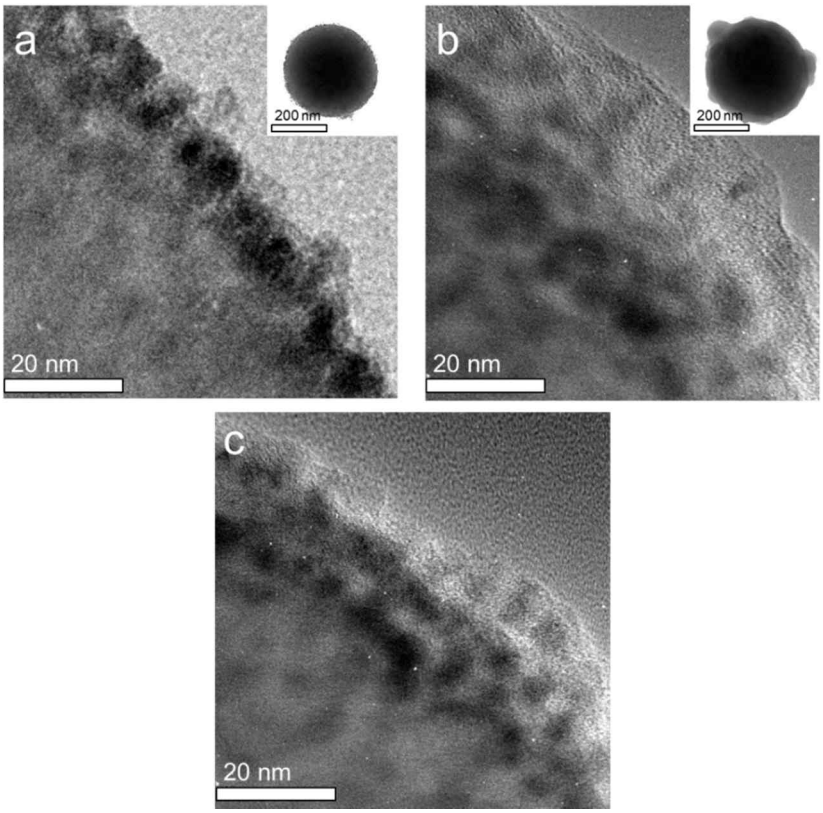

Figure 17. High resolution transmission electron microscopy (HR-TEM) images of QD-SiO_2 NP, PCDA immobilized SiO_2@QD NP, and PDA-QD-SiO_2 NP. Shell images of a) quantum dot (QD)-assembled silica nanoparticles (QD-SiO_2 NPs), b) QD-assembled silica NPs bearing PDA on their surface (PDA-QD-SiO_2 NPs) and c) PCDA immobilized QD-SiO_2 NPs. Inset: TEM images of single particle.[110]

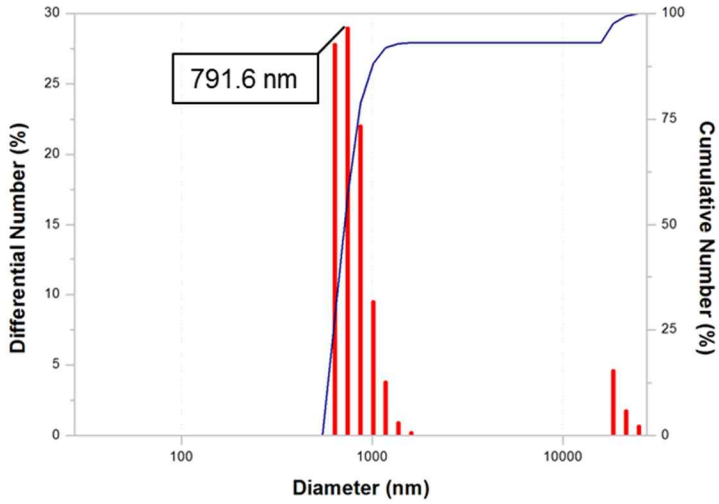

Figure 18. The size distribution of PDA-QD-SiO_2 NPs obtained by Dynamic Light Scattering (DLS) analysis. The NPs are diluted with ethanol.[110]

2.2. Optical Property Analysis

PDA shows unique color change from blue to red with fluorescence emission in response to a diverse external stimuli such as optical exposure, applied stress, ligand–receptor recognition, temperature and pH change.[116-118] The prepared PDA-QD-SiO_2 NPs were blue in color as shown in Fig. 19a. According to previous studies, blue-PDA does not emit fluorescence, whereas red and yellow-colored PDAs, induced by external stress including binding of target molecules, emit strong fluoresce.[114] Therefore, a turn-on response of PDA fluorescence enabled us to recognize whether a target exists or not if PDA contains the ligand for that target. We heated the bluePDA-QD-SiO_2 NPs at 100^{o}C for 5 min to confirm that the color change in response to an external stimulus. As shown in Fig. 19b, the color of bluePDA-QD-SiO_2 NPs changed to red (redPDA-QD-SiO_2 NPs), indicating that they were able to report the binding event through the color change. Once the target of interest is detected by the color change, the target can be easily identified via the fluorescence of the QD encoder.

Next, we investigated the optical properties of both bluePDA-QD-SiO_2 NPs and redPDA-QD-SiO_2 NPs to show that they can emit discrete PDA fluorescence for sensing and fluorescence of QDs for encoding without interference with each other. First, we analyzed the fluorescence images of the particles as shown in Fig. 20. Fig. 20a and 20b show the fluorescence images of blueQD-SiO_2 NPs and greenQD-SiO_2 NPs respectively, which exhibited bright photoluminescence (PL) with maxima at 490 and 540 nm, respectively. After introducing blue-PDA to the blueQD-SiO_2 NPs or greenQD-SiO_2 NPs, the color of the resulting particles (bluePDA-blueQD-SiO_2 NPs, bluePDA-greenQD-SiO_2 NPs) were identical with those particles without PDA (Fig. 20c and 20d), indicating that blue-PDA does not emit fluorescence. However, the fluorescence of redPDA-blueQD-SiO_2 NPs and redPDA-greenQD-SiO_2 NPs changed slightly to light sky-blue and dark green, respectively, due to the overlap of the two different fluorescence spectra produced from each QD and the red-PDA (Fig. 20e and 20f), clearly indicating that the red-PDA emits its own fluorescence (Fig. 20g). Then, we measured the fluorescence

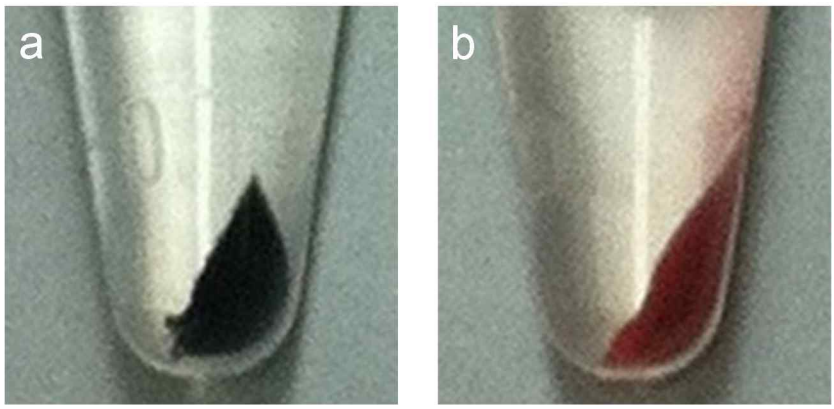

Figure 19. Photographs of a) bluePDA-QD-SiO_2 NPs and b) redPDA-QD-SiO_2 NPs.[110]

spectra of the PDA-QD-SiO_2 NPs. To achieve efficient multiplexed detection, each fluorophore sources should be spectrally distinguished at simultaneous excitation.[119,120] For this reason, those fluorophores need to emit at different wavelengths. As shown in Fig. 21a, blueQD-SiO_2 NPs and greenQD-SiO_2 NPs had discrete PL ranges without spectral overlap with that of redPDA-SiO_2 NPs, indicating that they can report both the existence of a target through PDA fluorescence and the kind of target through the PL of QDs during an assay. The redPDA-SiO_2 NPs emitted two broad fluorescent bands at 570 nm and 640 nm, which were identical to that of the red-PDA films or liposomes reported previously.[121] Fig. 21b and 21c show the fluorescence spectra of redPDA-blueQD-SiO_2 NPs and redPDA-greenQD-SiO_2 NPs, respectively. The PL of the QDs could be clearly distinguished from the red-PDA fluorescence. This result demonstrates that PDA-QD-SiO_2 NPs can reveal target information as well as the target binding event. The fluorescence intensity of the red-PDA was much lower than that of the QD (Fig. 22), which may be controlled by the amount of embedded QDs.

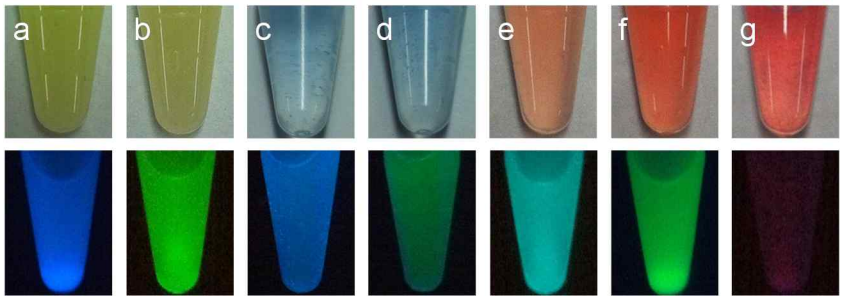

Figure 20. Photographs (top) and fluorescence images (bottom) of QD-SiO_2 NPs, PDA-QD-SiO_2 NPs and PDA-SiO_2 NPs. a) blueQD-SiO_2 NPs, b) greenQD-SiO_2 NPs, c) bluePDA-blueQD-SiO_2 NPs, d) bluePDA-greenQD-SiO_2 NPs, e) redPDA-blueQD-SiO_2 NPs, f) redPDA-greenQD-SiO_2 NPs and g) redPDA-SiO_2 NPs.[110]

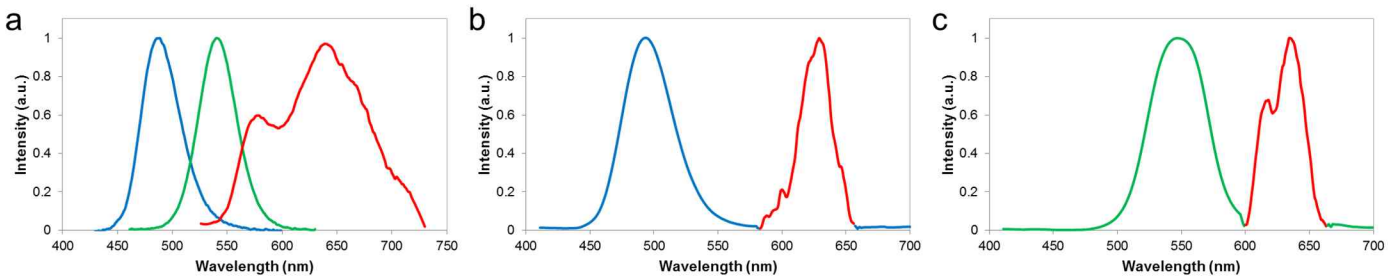

Figure 21. Photoluminescence spectra of a) blueQD-SiO_2 NPs (blue), greenQD-SiO_2 NPs (green), redPDA-SiO_2 NPs (red), b) redPDA-blueQD-SiO_2 NPs and c) redPDA-greenQD-SiO_2 NPs. Red lines in b) and c) are the fluorescence spectra emitted from the red-PDA. The fluorescence spectra of the QDs were normalized by their highest intensity at 493 nm (blue) and 540 nm (green), respectively, and the fluorescence spectra of red-PDA were normalized by their highest intensity at 630 nm, which were smoothed by the Savitzky–Golay method. See Fig. 18 for the original photoluminescence spectra.[110]

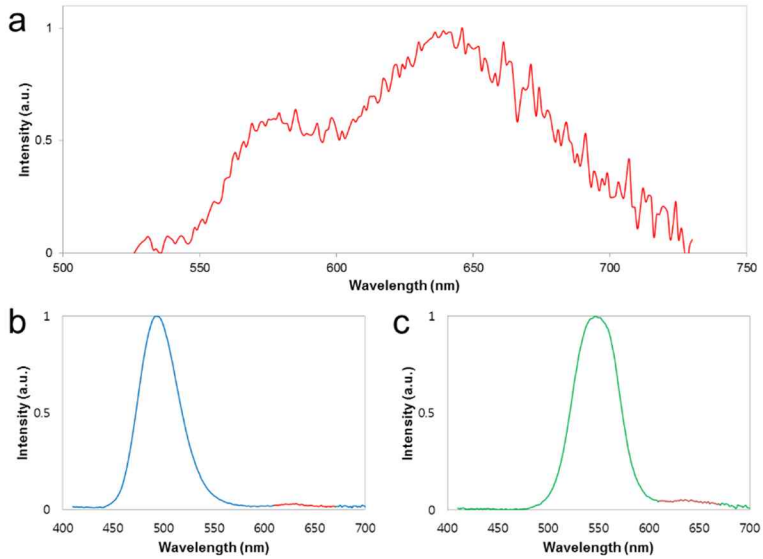

Figure 22. Photoluminescence spectra of a) redPDA-SiO_2 NPs, b) redPDA-blueQD-SiO_2 NPs and c) redPDA-greenQD-SiO_2 NPs. Red regions of b) and c) are the fluorescence spectra emitted from the red-PDA.[110]

2.3. Possibility of Multiplexed Optical Detection

To demonstrate the potential for label-free and multiplexed detection on PDA-QD-SiO_2 NPs, we mixed redPDA-blueQD-SiO_2 NPs and bluePDA-greenQD-SiO_2 NPs together in a 1:1 ratio in an aqueous solution and measured their fluorescence using image restoration microscopy (IRM) with an RD-TR-PE filter (617 nm), a DAPI filter (457 nm), and a YFP filter (535 nm). As shown in Fig. 23, the red fluorescence image (Fig. 23b) was clearly observed under the red filter (RD-TR-PE, emission: 617/73 nm), which was produced from red-PDA on redPDA-blueQD-SiO_2 NPs (Fig. 23a). In addition, a blue fluorescence image produced from the QDs of redPDA-blueQD-SiO_2 NPs was obtained under a blue filter (DAPI, emission: 457/50 nm), as shown in Fig. 23c. If we assume that the red-PDA fluorescence was caused by binding of the target molecule on the bluePDA-blueQD-SiO_2 NPs, we could easily detect the target through the turn-on signal of the fluorescence emitted from the red-PDA. Additionally, the target molecule could

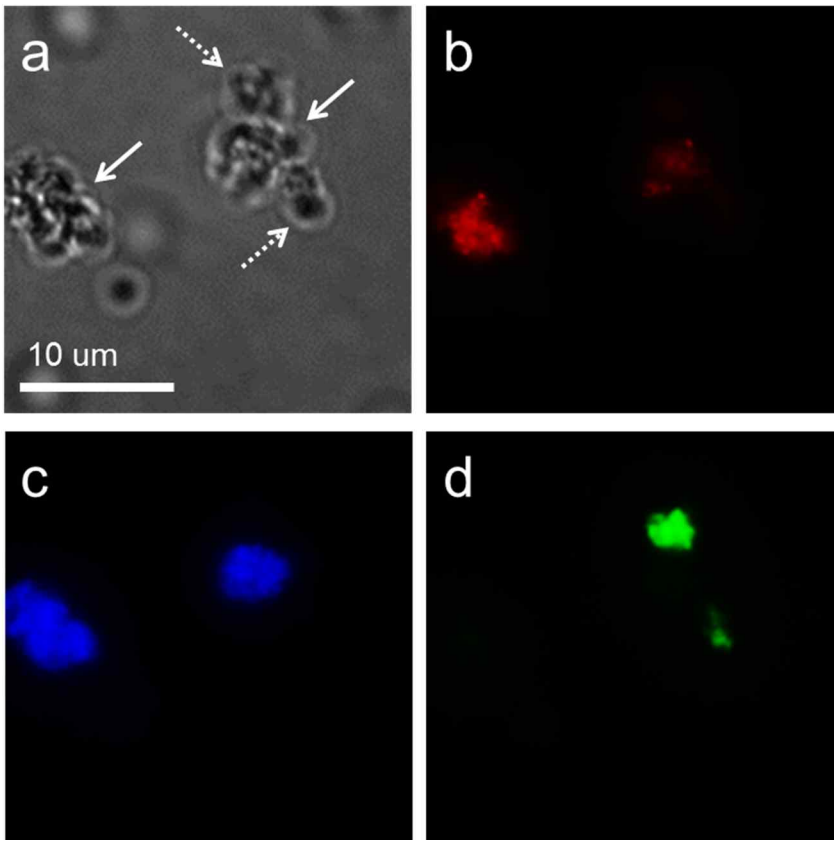

Figure 23. Microscopic images of redPDA-blueQD-SiO_2 NPs and bluePDA-greenQD-SiO_2 NPs mixture. a) Optical image, b) fluorescence image of the NPs under a red filter (RD-TR-PE, emission: 617/73 nm), c) under a blue filter (DAPI, emission: 457/50 nm), d) a under green filter (YFP, emission: 535/20 nm).[110]

be readily identified via the blue PL of the QDs. When there is no target molecule in the sample, the red fluorescence of the PDA would not be observed, whereas the green PL of the QDs in bluePDA-greenQD-SiO_2 NPs (striped arrow at Fig. 19a) for encoding would still remain bright (Fig. 23d). These results clearly demonstrate the potential of PDA-QD-SiO_2 NPs system for label-free, multiplexed detection of target molecules in a bioassay, as shown in Fig. 24.

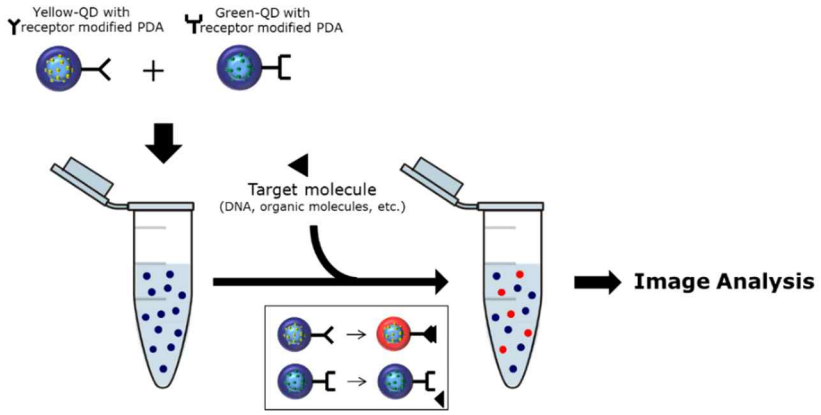

Figure 24. Schematic illustration of multiplexed and label-free biomolecule detection using PDA-QD-SiO_2 NPs.

3. Conclusion

We have demonstrated the possibility of using QD-assembled silica NPs coated with a PDA supramolecule for label-free, multiplexed detection of target molecules. PDA-QD-SiO_2 NPs emitted a discrete range of fluorescence from a PDA layer and from QDs without overlap or quenching. The fluorescence of PDA on the PDA-QD-SiO_2 NPs was effectively turned on in response to an external stress, which was successfully imaged and readily distinguished from nonfluorescent NPs using fluorescence microscopy.

Chapter III. Fabrication of Monodispersed Silica-Coated Quantum Dot-Assembled Magnetic Nanoparticles

1. Experimental Section

1.1. Chemicals and Materials

All chemicals were used as received without further purification. A dispersion of Fe_3O_4 NPs (18 nm in average diameter, oleate-stabilized in toluene) was purchased from Ocean Nanotech, USA. Polyvinylpyrrolidone (PVP-10K), tetraethyl orthosilicate (TEOS), and 3-mercaptopropyltriethoxysilane (MPTS) were purchased from Sigma-Aldrich, Korea. Diethyl ether (anhydrous), dimethylformamide (DMF), dichloromethane (DCM), ethanol (EtOH), and ammonia aqueous solution (27%) were obtained from Daejung Pharm, Korea. A dispersion of QDs (core-multishell structure composed of CdSe@CdS@ZnS, ca. 4.5 nm in average diameter, oleate-stabilized in toluene) was purchased from Nanosquare, Korea.

1.2. Preparation of Silica-Coated F_3O_4 NPs

Ligand Exchange of Oleate-Stabilized Fe_3O_4 NPs with Polyvinylpyrrolidone (PVP)

A 0.2-mL mixture of oleate-stabilized Fe_3O_4 NPs in toluene was transferred to a 10-mL vial and diluted with 5 mL of DMF-DCM (1:1, v/v). Then, 60 mg of PVP was added and stirred overnight at 100°C. After the reflux, the reaction mixture was added to diethyl ether (10 mL), and subsequently precipitated to obtain PVP-stabilized Fe_3O_4 NPs. The precipitate was centrifuged at 4500 rpm for 5 min and then transferred to 6.5 mL of EtOH to facilitate the formation of a stable dispersion of Fe_3O_4 NPs.

Silica Coating on PVP-Stabilized Fe_3O_4 NPs

Silica coating procedure on PVP-stabilized Fe_3O_4 NPs was followed by a modified Stöber method. A 0.28-mL solution of ammonia aqueous solution was added to the EtOH dispersion of PVP-stabilized Fe_3O_4 NPs (6.5 mL), followed by the addition of

TEOS (6.5 μL). The reaction mixture was stirred overnight at 25°C. The silica-coated Fe_3O_4 NPs were then centrifuged at 10,000 rpm for 1 h, washed repeatedly with EtOH, and re-dispersed in distilled water. A 4 mL solution of TEOS in EtOH (3 vol%) was added to the silica-coated Fe_3O_4 NPs (M-SiO_2 NPs) dispersion, and then stirred for one day. The resulting M-SiO_2 NPs were centrifuged at 7,000 rpm for 10 min and re-dispersed in EtOH.

1.3. Preparation of Silica-Coated Quantum Dot-Assembled Magnetic Nanoparticles (M-QD-SiO_2 NPs)

Thiol groups were introduced to the surface of M-SiO_2 NPs (5 mL, 0.6 mg/mL suspension in EtOH) by adding MPTS (25 μL) and ammonia aqueous solution, and followed by stirring overnight at 25°C. These thiol-functionalized M-SiO_2 NPs were then washed three times with EtOH and re-dispersed in EtOH. The resulting NPs (1 mL, 10 mg/mL in EtOH) were subsequently added to olleic acid-coated QDs containing DCM solution (4 mL, 1.75 mg/mL), and vigorously stirred for 3 min. Subsequently, MPTS (55 μL) and ammonia aqueous solution were added to the M-QD-SiO_2 NPs mixture, and shaken for 1 h at 25°C. The resulting mixtures were then washed with EtOH, dispersed in EtOH (5 mL) containing TEOS (55 μL) and ammonia aqueous solution (55 μL), and stirred overnight. The resulting M-QD-SiO_2 NPs were washed three times with EtOH and subsequently dispersed in EtOH.

1.4. Analysis of NPs

Physical Property

Transmission electron microscopy (TEM) analysis was performed on a Libra 120 (Carl Zeiss, Germany) operating at 120 kV. All the samples for TEM analysis were deposited on a 300 mesh holey carbon grid. Hydrodynamic size and degree of dispersion of the NPs were determined using a Nanosight LM10. All the samples for DLS analysis were dispersed in EtOH.

Optical and Magnetic Property

Ultraviolet-visible (UV-Vis) absorption spectra were obtained with an Optigen 2120UV. Photoluminescence (PL) spectra were obtained with a Perkin-Elmer LS55. The QY of prepared NPs was obtained with a JASCO FP-6500, equipped with an integrating sphere and a QY calculation program. The fluorescence decay of prepared NPs was obtained with time-correlated single photon counting (TCSPC) technique using 405 nm diode laser at a

repetition rate of 10 MHz.

Field-dependent magnetization of the Fe_3O_4–based NPs was performed with a Quantum Design PPMS-14.

1.5. Confocal Laser Microscopy and Flow Cytometric Analysis

Confocal Laser Microscopic Analysis

For confocal microscopy analysis, MDA-MB-231 cells (1×10^5) were seeded on clean coverslips in a 6-well plate, followed by incubation at 37ºC for 24 h. The cells were rinsed with phosphate buffered saline (PBS), treated with M-QD-SiO_2 NPs (40 μg/mL in PBS), and incubated at 37ºC for 1 h. The cells treated with M-QD-SiO_2 NPs were fixed by treating with 4% paraformaldehyde solution (Affymetrix, USA) for 15 min. The cells were thoroughly washed three times with PBS and attached to the coverslip using a mounting solution containing 4′,6-diamidino-2-phenylidole (DAPI) solution (Vector Laboratories, USA). Confocal microscopy images were obtained using a Zeiss LSM 510.

Magnetic Field-Assisted Cell Separation and Flow Cytometric Analysis

For magnetic separation of NP-treated cells, each of the two

types of NPs, namely, non-magnetic redQD-SiO_2 NPs and magnetic M-greenQD-SiO_2 NPs (40 μg/mL in PBS), were incubated with MDA-MB-231 cells at 37ºC. After 1 h, the NPs-treated cells were harvested and combined. A magnet was located on 1 mm distance of the well plate, and the floating cells were incubated with the magnet at room temperature for 4 h. After an additional 24 h of incubation at 37ºC in the absence of the magnet, the cells were fixed and analyzed with confocal microscopy. Flow cytometric analysis (BD FACS Calibur-2, USA) was performed with a cell mixture composed of the same numbers of redQD-SiO_2 NPs-internalized and M-greenQD-SiO_2 NPs-internalized cells. The mixture was analyzed by laser excitation at 488 nm, with 530/30 nm and 661/16 nm emission filters.

2. Results and Discussion

2.1. Preparation of M-QD-SiO_2 NPs

M-QD-SiO_2 NPs (Fig. 25) were prepared from M-SiO_2 NPs, which were synthesized by using the method described previously.[122] Briefly, the M-SiO_2 NPs were prepared by encapsulating Fe_3O_4 NPs with a silica layer by a modified Stöber method [123]. First, amphiphilic PVP was used to replace oleic acid as the surface ligand of the Fe_3O_4 NPs (18 nm in average diameter) to obtain a hydrophilic surface. As shown in Fig. 26a and 26b, the size and shape of the Fe_3O_4 NPs remained unchanged during the ligand exchange process. The M-SiO_2 NPs were formed after reacting with TEOS and ammonium hydroxide, as shown in the TEM image of Fig. 26c. The resulting NPs have a magnetic core and silica shell, exhibiting uniform average particle size (75 ± 2.6 nm) and hydrodynamic size (~200 nm) (Fig. 27a). The size distribution of the prepared NPs were determined from TEM images of randomly selected 50 samples.

Ligand exchange method was applied to immobilize the oleic

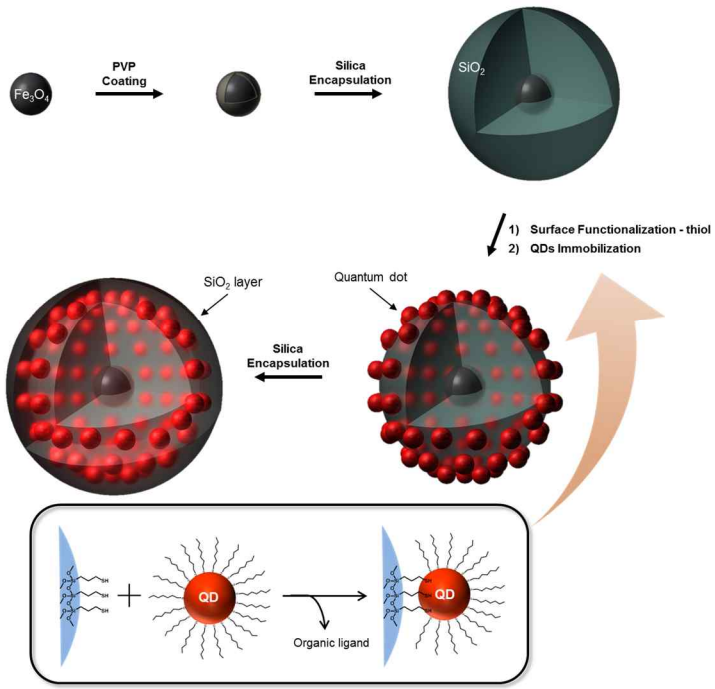

Figure 25. Illustration of the synthesis of M-QD-SiO_2 NPs.[124]

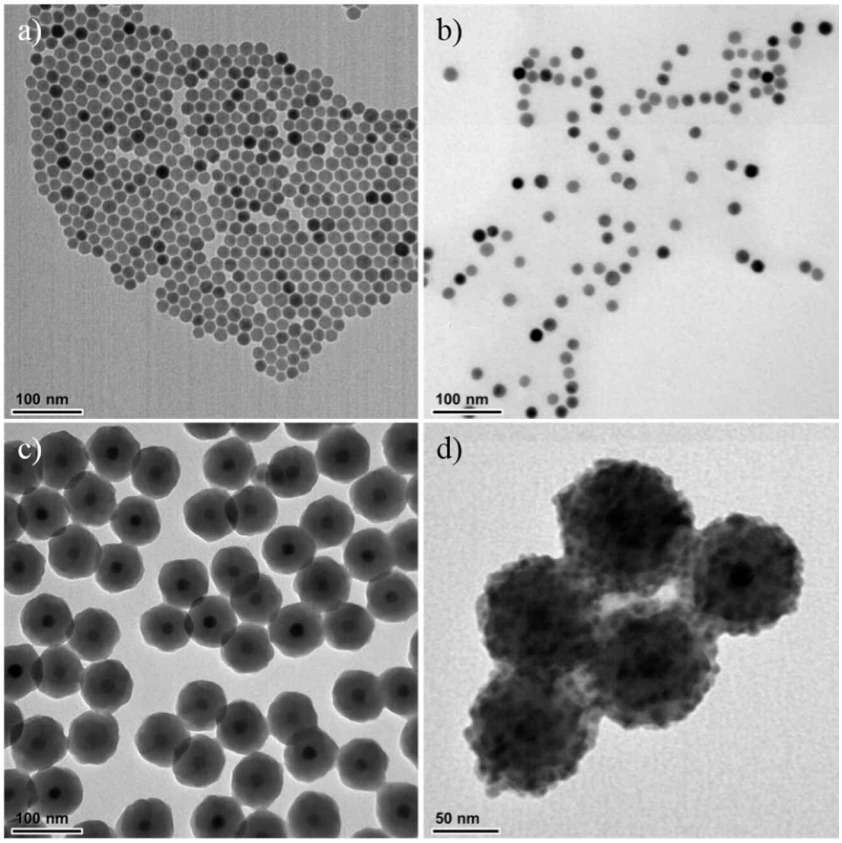

Figure 26. TEM images of NPs at each step of the synthesis. a) Oleate-coated Fe_3O_4 NPs, b) PVP-coated Fe_3O_4 NPs, c) M-SiO_2 NPs, d) M-QD-SiO_2 NPs.[124]

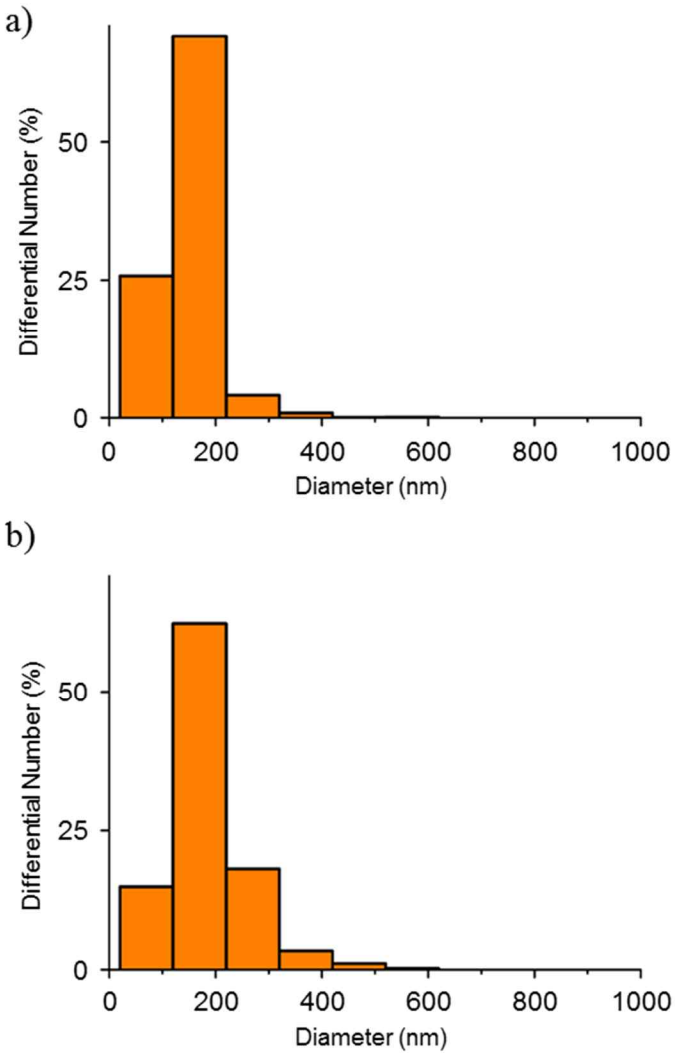

Figure 27. Hydrodynamic size distribution analysis of NPs. a) M-SiO_2 NPs, b) M-QD-SiO_2 NPs.[124]

acid-coated CdSe@CdS@ZnS QDs onto the silica surface. For this, we introduced thiol groups which is well known to have strong coordination ability with metal surface such as metal oxides [125], InP [126] and metal sulfides.[127] The M-SiO_2 NPs were functionalized with a thiol silane coupling monomer, MPTS, for facile immobilization of the CdSe@CdS@ZnS QDs. The QDs immobilization and silica shell addition were performed by using the same method previously described.[107] First, controlled amounts of EtOH solution containing the thiol-functionalized M-SiO_2 NPs and DCM solution containing QDs were mixed. The thiol groups of M-SiO_2 NPs interacted with the Zn atoms on the surface of CdSe@CdS@ZnS QDs, replacing organic ligands.[16] Subsequently, MPTS was added to the QDs-immobilized M-SiO_2 NPs to replace the remained organic ligands and hydrolyzed into silanol groups, forming thin silica-shell precursor on the surface of NPs. The QDs were embedded in the surface of silica as *ca.* 0.9 unit per 100 nm^2, which is more QD-densed structure compared to the QD-SiO_2 NPs. The NPs were then encapsulated with a silica shell by TEOS. As shown in Fig. 22d, the size of M-QD-SiO_2 NPs was ~100 nm,

which is slightly larger than that of bare Fe_3O_4@SiO_2 NPs. Slight increase of the size is due to the addition of QDs and additional silica shell layer on the surface. Significant aggregation of NPs was not detected (Fig. 23b) and the obtained NPs were uniform in size (97 ± 4.8 nm).Three types of NPs were fabricated through this procedure. Two types of QDs, which have fluorescence emission maxima at 620 nm and 540 nm respectively, were used in this study. The NPs which contain "red-QDs" were fabricated using QDs which have emission maxima at 620 nm, and other NPs which contain "green-QDs" were fabricated using QDs which have emission maxima at 540 nm.

Table 2. Classification of the fabricated M-QD-SiO_2 NPs

Nanoparticles	Structure of exploited QDs	Emission peak of QD fluorescence	Structure of silica NPs
redQD-SiO_2 NPs	CdSe@CdS @ZnS	620 nm	Bare SiO_2 NPs[a]
M-redQD-SiO_2 NPs	CdSe@CdS @ZnS	620 nm	Fe_3O_4@SiO_2 NPs[b]
M-greenQD-SiO_2 NPs	CdSe@CdS @ZnS	540 nm	Fe_3O_4@SiO_2 NPs[b]

a : NPs were fabricated using general Stöber method[123]

b : NPs were fabricated using by encapsulating PVP-coated Fe_3O_4 NPs[122]

2.2. Optical Property of M-QD-SiO_2 NPs

The fluorescence properties of the NPs were analyzed. The M-redQD-SiO_2 NPs and M-greenQD-SiO_2 NPs were excited at 350 nm wavelength using a xenon lamp. Both of them exhibited bright photoluminescence with emission maxima at 620 and 540 nm (Fig. 24a) respectively, which are identical with the original single QDs (Fig. 24b). The QY of the prepared NPs was obtained with a JASCO FP-6500, equipped with an integrating sphere and a QY calculation program. The prepared NPs were excited by a light source of 450 nm wavelength, and the measured number of irradiated/luminescent photons and the ratio of absorbed photons were analyzed by the following equation.

$$Quantum\ \ yield\ \ (\%) = \frac{Number\ of\ luminescent\ \ photons}{Number\ of\ absorbed\ \ photons}$$

$$= \frac{Number\ of\ luminescent\ \ photons}{Number\ of\ irradiated\ \ photons \times ratio\ \ of\ absorbed\ \ photons}$$

The original red QDs in DCM solution had QY of 86%. The QY

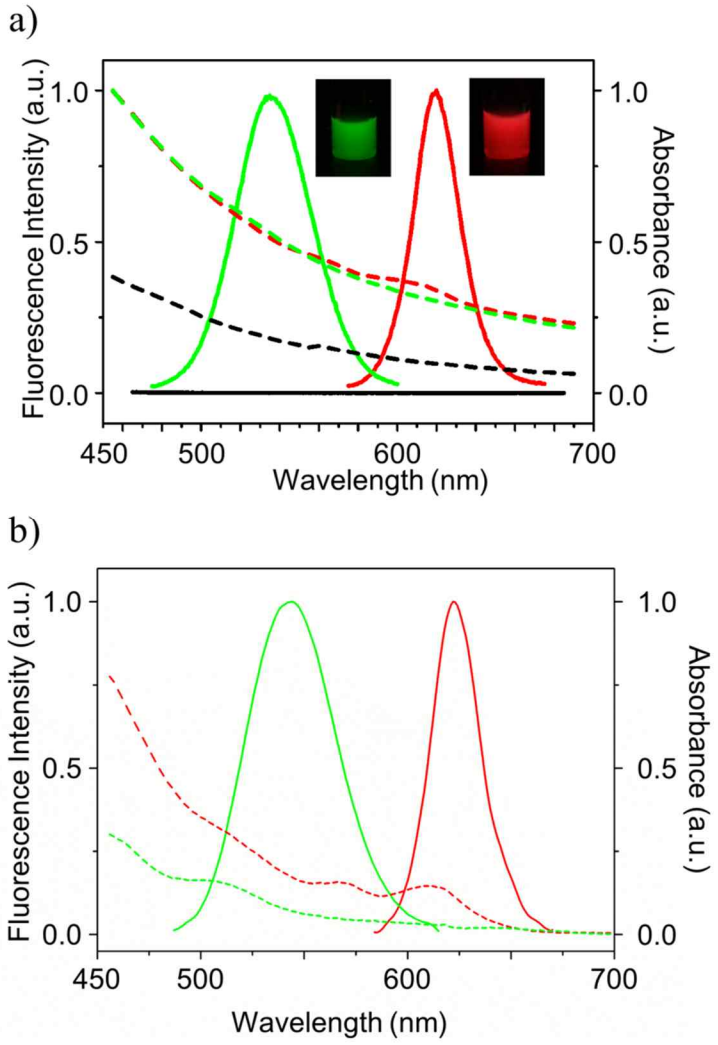

Figure 28. Optical property of M-QD-SiO_2 NPs and single QDs. UV absorption (dashed line) and fluorescence emission (straight line) spectrum of (a) red and green QDs-embedded M-QD-SiO_2 NPs (red and green lines) and M-SiO_2 NPs (black line) (inset: photographs of M-greenQD-SiO_2 NPs and M-redQD-SiO_2 NPs) and (b) the original red and green QDs.[124]

of the M-redQD-SiO_2 NPs was determined to be 57%, which is slightly less than that (71%) of the bare redQD-SiO_2 NPs. The QY of original green QDs in DCM solution was quantified as 70%, and the QY of greenQD-SiO_2 NPs and M-greenQD-SiO_2 NPs were 63% and 40%, respectively. Since the M-SiO_2 NPs have a broad absorption spectrum in the UV and visible range, both excitation light source and QDs fluorescence could be absorbed by Fe_3O_4 NPs. Furthermore, as the absorption of Fe_3O_4 NPs decreases in the longer wavelength, the smaller loss of QY in M-redQD-SiO_2 NPs than M-green-SiO_2 NPs could be explained.[128,129]

To clarify if other factors are involved for giving the QY differences between the M-QD-SiO_2 NPs and QD-SiO_2 NPs, TCSPC detection was carried out. As shown in Fig. 29, M-QD-SiO_2 NPs show short fluorescence lifetime compared to QD-SiO_2 NPs. In general, the reduction of fluorescence lifetime is mainly caused by various non-radiational energy transfer processes including Förster resonance energy transfer (FRET).[130,131] For M-QD-SiO_2 NPs, there are two possible fluorescence acceptors for these process. First, Fe_3O_4 NP in the center of M-QD-SiO_2 NP

could be considered as an energy acceptor against QDs fluorscence. Fe_3O_4 NPs associated FRET as an acceptor has been widely studied so far.[132,133] However, it is hard to be applied for M-QD-SiO_2 because FRET requires short distance between donor and acceptor, within 10 nm.[42,134,135] The distance between QDs and Fe_3O_4 NP in M-QD-SiO_2 is *ca.* 30 nm. Secondly, the densely packed QDs on the surface of M-QD-SiO_2 NPs could act as energy acceptors to the adjacent QDs and reduce the fluorescence lifetime.[136] Since M-QD-SiO_2 NP had higher density of QDs per surface area (~ 0.9 unit/100 nm^2) compared to that of QD-SiO_2 NP (~ 0.7 unit/100 nm^2), the fluorescence lifetime reduction could be properly explained.

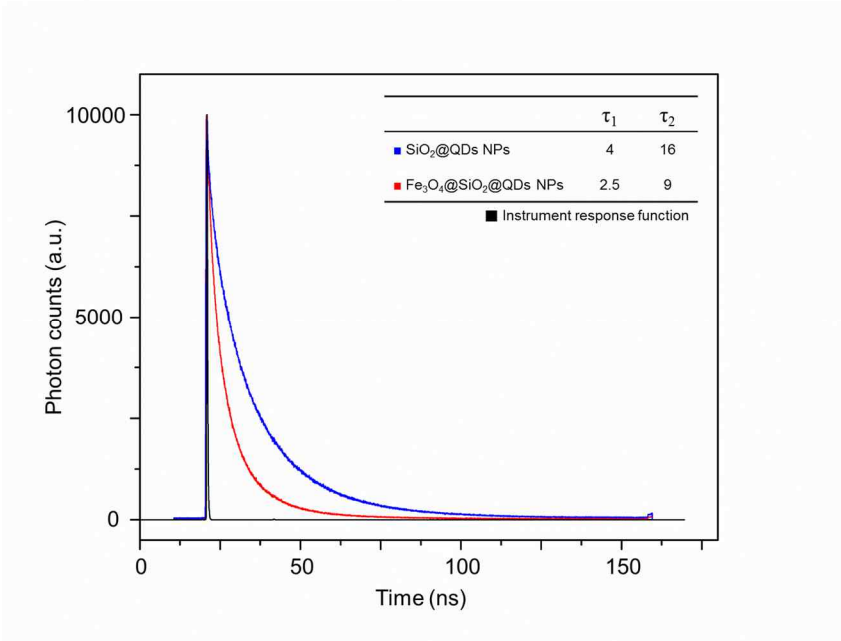

Figure 29. Fluorescence decay (405 nm excitation) of redQD-SiO_2 NPs (blue) and M-redQD-SiO_2 NPs (red) monitored at 583/75 nm and the corresponding instrument response function. The decays were fitted using a multi-exponential function and exhibited at least two distinct lifetimes (τ_1 and τ_2).[124]

2.3. Magnetic Property of M-QD-SiO_2 NPs

The magnetic properties of the M-QD-SiO_2 NPs were also measured to demonstrate that they can be employed for cell separation. The field-dependent magnetism of the M-QD-SiO_2 NPs at 300 K exhibited super-paramagnetic characteristics (Fig. 26), with a saturated magnetization of ~1.25 emu/g. Furthermore, the NPs could be collected easily using a NdFeB magnet (Fig. 27a) and then clearly re-dispersed under gentle agitation. After agitation, the M-QD-SiO_2 NPs were found to be well-dispersed in various hydrophilic solvents (Fig. 27b) owing to their hydrophilic silica surface.

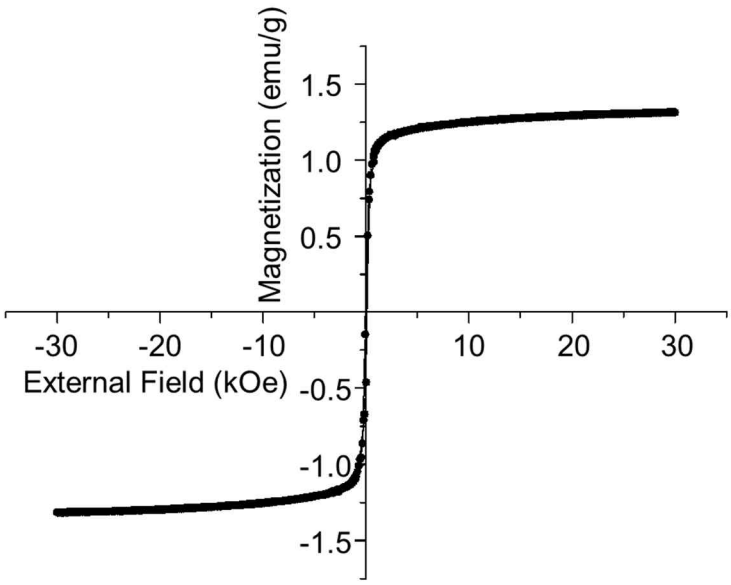

Figure 30. Hysteresis loop of M-QD-SiO_2 NPs.[124]

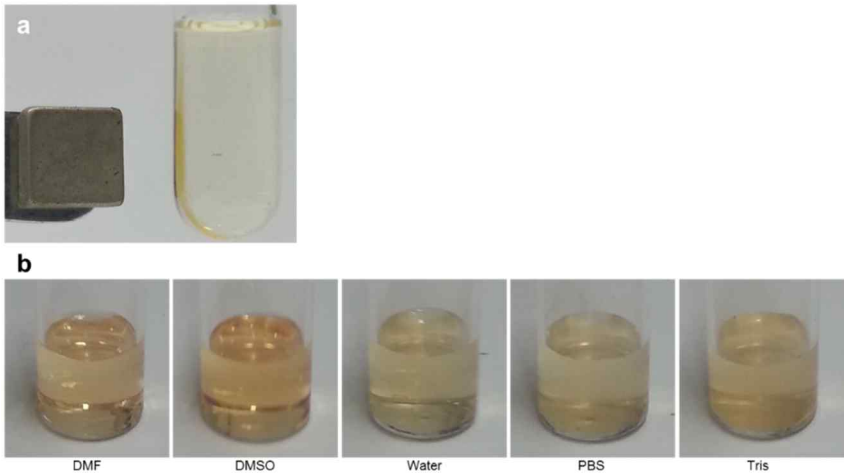

Figure 31. a) NP separation using NdFeB Magnet, b) dispersed M-QD-SiO_2 NPs in various solvents.[124]

2.4. Magnetic Field-Assisted Cell Separation

To show that the M-QD-SiO_2 NPs could be exploited for cell separation, in vitro analysis was subsequently performed using both fluorescence and magnetic field. The natural cell uptake of the prepared NPs was confirmed by incubating MDA-MB-231 human breast cancer cells with M-QD-SiO_2 NPs at 37^{o}C for 1 h. Confocal microscopy images (Fig. 28a) confirmed that most of M-QD-SiO_2 NPs were accumulated in the cytoplasm of the cells by natural endocytosis. In order to verify the applicability of M-QD-SiO_2 NPs in FACS experiments, cells containing red or green QDs-embedded NPs were then analyzed using flow cytometry. Each cell was excited by a 488-nm laser source. As shown in the scatter plots Fig. 28b, the cells can be clearly distinguished with the 661/16 nm and 530/30 nm emission filters. These results indicate that cells containing M-QD-SiO_2 NPs are suitable to use with flow cytometry.

Furthermore, the ability of the M-QD-SiO_2 NPs for use in magnetic separation was confirmed. Thus, cells that had

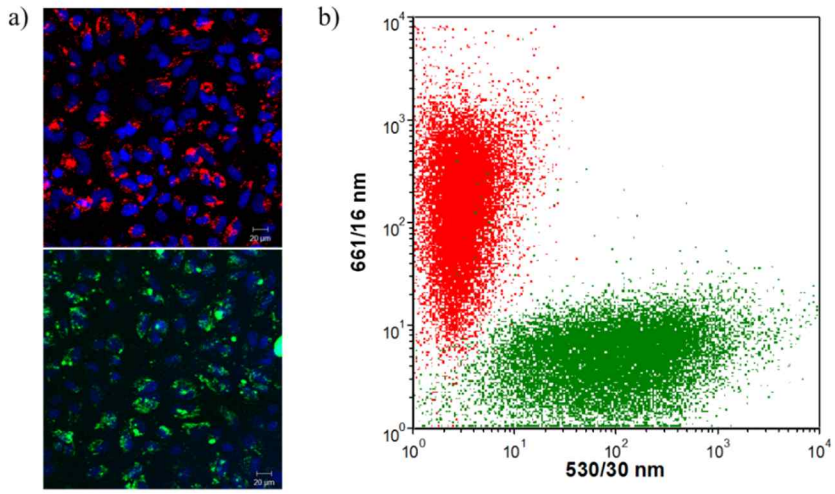

Figure 32. Cellular internalization assessment of M-QD-SiO_2 NPs. a) Fluorescence images of MDA-MB-231 cells that internalized M-redQD-SiO_2 NPs (upper panel) and the cells that internalized M-greenQD-SiO_2 NPs (lower panel). b) Scatter plot of the fluorescence-activated cell sorting (FACS) analysis of the cells that had internalized either M-redQD-SiO_2 NPs or M-greenQD-SiO_2 NPs.[124]

internalized non-magnetic redQD-SiO_2 NPs or M-greenQD-SiO_2 NPs were mixed in equal amounts and placed on a 6-well plate near a NdFeB magnet for 4 h. The regions of the plate adjacent to and distant from the magnet were simultaneously excited by a 405-nm laser and examined using confocal microscopy. As shown in Fig. 29, the cells that contained M-greenQD-SiO_2 NPs were mostly observed in regions near the magnet, while the cells that contained non-magnetic redQD-SiO_2 NPs were located at the region distant from the magnet; i.e., most of the magnetized cells were accumulated close to the magnet. These results demonstrate the potential use of the M-QD-SiO_2 NPs in magnetic field-assisted cell separation.

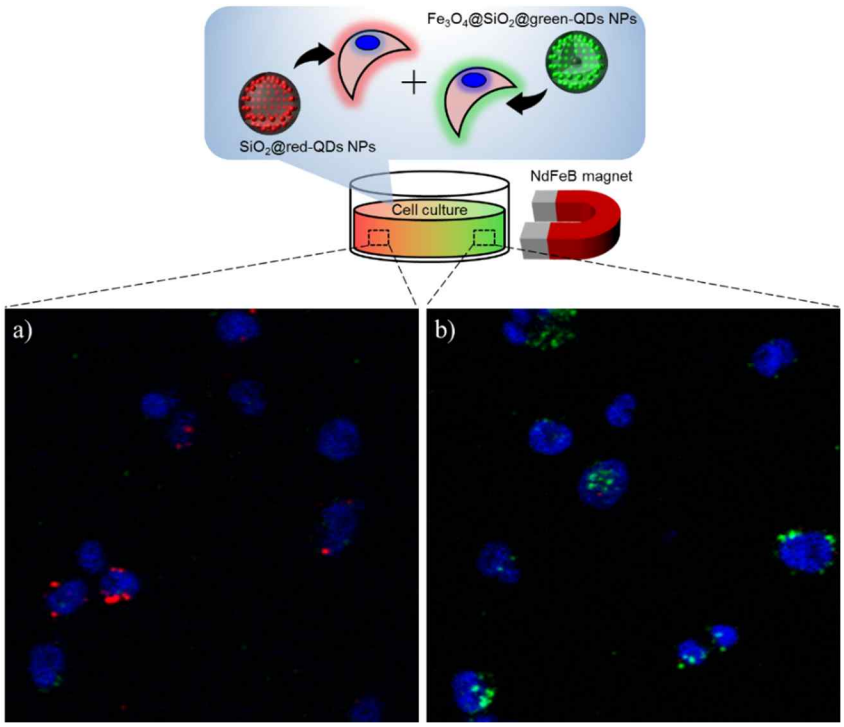

Figure 33. Illustration of magnetic field-assisted cell separation using M-QD-SiO_2 NPs and microscopic images of the separated cells containing either magnetic M-greenQD-SiO_2 NPs or nonmagnetic redQD-SiO_2 NPs. Sample plate regions a) adjacent to and b) distant from the magnet.[124]

3. Conclusion

Multifunctional NPs of uniform size that have strong fluorescence and super-paramagnetic properties were fabricated by immobilizing QDs onto the surface of silica-coated iron oxide NPs. The applicability of M-QD-SiO_2 NPs in flow cytometry and magnetic-assisted cell separation was demonstrated. Our results prove that M-QD-SiO_2 NPs have a great potential for use in biomedical applications, particularly for multimodal cell separation.

Chapter IV. Fabrication of Superparamagnetic Iron Oxide Nanoparticles-Assembled Nanosphere for Bioapplication

1. Experimental Section

1.1. Chemicals and Materials

All chemicals were used as-received without further purification. A dispersion of Fe_3O_4 NPs (mean diameter, 18 nm, oleate-stabilized in chloroform) was purchased from Ocean Nanotech (Springdale, AR, USA). Polyvinylpyrrolidone (PVP-10K), tetraethyl orthosilicate (TEOS), 3-aminopropyltriethoxysilane (APTS), succinic anhydride, dopamine hydrochloride, biotin, streptavidin-conjugated fluorescein isothiocyanate (streptavidin-FITC), *N*-hydroxysuccinimide (NHS), 4-dimethylaminopyridine (DMAP), and *N,N'*-diisopropylcarbodiimide (DIC) were purchased from Sigma-Aldrich (St. Louis, MO, USA). Diethyl ether (anhydrous), dimethylformamide (DMF), dichloromethane (DCM), ethanol (EtOH), isopropyl alcohol (IPA), and ammonium hydroxide (28 wt% in water) were obtained from Daejung Chemicals (Daejeon, Korea). *N,N*-Diisopropylethylamine (DIEA) was purchased from Alfa Aesar (Ward Hill, MA, USA). Absolute ethanol (99.5%, HPLC grade) was purchased from Carlo Erba

(Milan, Italy). 2-(1*H*-Benzotriazole-1-yl)-1,1,3,3-tetramethyl uronium hexafluorophosphate (HBTU) and hydroxybenzotriazole hydrate (HOBt) were purchased from Beadtech (Seoul, Korea).

Mouse embryonic fibroblast cell line NIH 3T3, human caucasian prostate adenocarcinoma cell line PC-3, human glioblastoma astrocytoma cell line U-87 MG were obtained from the Korean Cell Line Bank (Seoul, Korea). All cells were cultured at 37 °C with 5% CO_2 under fully humidified conditions, supplemented with 10% fetal bovine serum (FBS) (Invitrogen, Grand Island, NY, USA), 10 U/mL of penicillin (Invitrogen, Grand Island, NY, USA), and 10 μg/mL of streptomycin.

1.2. Preparation of Single-Layer (SL M-SiO_2 NPs) and Double-Layer Magnetic Nanoparticle-Embedded Silica Nanospheres (DL M-SiO_2 NPs)

Synthesis of Dopamine-Conjugated SiO_2 NPs

The synthetic procedure of SiO_2 NPs was previously described in Chapter 1. Amine groups were introduced to the SiO_2 NPs (2 mg/mL, 20 mL in EtOH) with APTS (100 μL) and ammonium hydroxide (100 μL) for 18 h. The reaction mixture was centrifuged at 7,000 rpm for 15 min, and the resulting SiO_2 NPs were washed several times with EtOH, and re-dispersed in DMF. The amine-functionalized SiO_2 NPs (2 mg/mL, 20 mL in DMF) were reacted with succinic anhydride (40 mg) and DIEA (40 μL). The reaction mixture was stirred for 3 h and washed with DMF several times by centrifugation. The carboxyl group ended-SiO_2 NPs (2 mg/mL, 20 mL in DMF) were reacted with dopamine hydrochloride (56 mg) and the two equivalent of HOBt, HBTU, and DIEA for 3 h. The dopamine-loaded SiO_2 NPs were washed several times with DMF by centrifugation (7,000 rpm for 15 min) and redispersed in DMF.

Ligand Exchange of Oleate-Stabilized Fe_3O_4 NPs with PVP

The ligand exchange procedure of oleate-stabilized Fe3O4 NPs with PVP was previously described in Chapter 3.

Preparation of Single-Layer and Double-Layer Magnetic Nanoparticle-Embedded Silica Nanospheres

Dopamine-conjugated SiO_2 NPs (0.2 mg/mL DMF, 5 mL in DMF) were poured into a PVP-stabilized Fe_3O_4 NPs solution (0.14 mg/mL, 5 mL in EtOH) and sonicated for 1 h. The reaction mixture was centrifuged at 7,000 rpm for 10 min, and washed three times with IPA and dispersed in IPA. TEOS (50 μL) and ammonium hydroxide (125 μL) were added to the Fe_3O_4 NPs-immobilized SiO_2 NP suspension (0.2 mg/mL, 5 mL in IPA) and stirred for 18 h. The reaction mixture was centrifuged and washed several times with EtOH and dispersed in EtOH. The DL MNPs were synthesized from SL MNPs by repeating the same process.

1.3. Characterization of SL M-SiO_2 NPs and DL M-SiO_2 NPs

Physical Property Analysis

Transmission electron microscopic (TEM) images of the prepared NPs were obtained with a JEOL JEM1010 (Tokyo, Japan) for normal use and with a JEOL JEM 3010 (Tokyo, Japan) for high resolution analysis, respectively. Hydrodynamic size and the degree of dispersion of the NPs were determined by using the dynamic light scattering spectrometer, Nanosight (LM10). Fluorescence microscopic images were obtained with a Perkin-Elmer LS55 instrument (Waltham, MA, USA). Field-dependent magnetization of the DL M-SiO_2 NPs was measured with the Quantum Design PPMS-14 instrument.

Magnetic Property Analysis

Three types of NPs (SL M-SiO_2 NPs, DL M-SiO_2 NPs, and silica-coated Fe_3O_4 NPs) were dispersed in a 50 mL tube with

EtOH. The NPs were attracted with a NdFeB magnet, and a 10 μL aliquot of solution was harvested at 0, 1, 2, 3, 5, 10, and 30 min. The concentrations of the initial and harvested NPs were analyzed using Nanosight LM10.

Stability Test

A 0.25 mg portion of SL M-SiO_2 NPs was added to three kinds of buffer solutions; pH 4.0 potassium hydrogen phthalate buffer (50 mM, 1 mL), pH 7.0 potassium hydrogen phosphate buffer (50 mM, 1 mL), and pH 10 sodium borate buffer (50 mM, 1 mL), respectively. After storage for one week at 25˚C, the NP samples were collected for analysis.

For stability analysis in cell culture medium, a 0.25 mg portion of the SL M-SiO_2 NPs was added into cell culture medium (10% FBS, 10 U/mL of penicillin, and 10 μg/mL of streptomycin) and tested for 7 days at 4˚C.

Cell Viability Analysis

Three types of cell lines, NIH 3T3, PC-3 and U-87 MG, were inoculated at conctration of 5×10^3 cells in a 96-well microplate, respectively, and DL M-SiO_2 NPs of increasing concentration, ranging from 25 to 200 μg, were transferred to each of the seeded cells. After incubation for 24 h at 37°C, the cellular toxicity was examined using a simple cellular toxicity kit, cell counting kit-8 (CCK-8) (Dojindo Molecular Tech, Inc, Rockville). The incubated cell medium was clearly removed via a phosphate buffered saline (PBS) washing step, and 10 μ L of the CCK-8 solution containing fresh cell medium were placed into each 96-well microplate. After incubation of the CCK-8-treated samples for 2 h, their absorbance at 450 nm was recorded using a microplate reader.

1.4. Magnetic Field-Assisted Protein Separation

DL M-SiO_2 NPs (0.2 mg/mL, 5 mL in EtOH) were reacted with APTS (50 μL) and ammonium hydroxide (50 μL) at room temperature for 12 h. The reaction mixture was washed several times with EtOH and re-dispersed in DMF. The resulting amine-functionalized NPs (1 mg/mL, 1 mL in DMF) were reacted with biotin (2.44 mg) and the same equivalent of HBTU, HOBT, and a two equivalent of DIEA for 3 h. The reaction mixture was washed several times with DMF and redispersed in PBS buffer (10 mM, pH 7.4). The biotin-conjugated DL M-SiO_2 NPs (1 mg/mL, in 1 mL PBS) were mixed with a streptavidin-FITC conjugate (5 mg/mL, 20 μL) and stirred for 1 h. Then, the mixture was washed three times with PBS buffer. The streptavidin captured M-SiO_2 NP suspension was collected using a NdFeB magnet, and resuspended in fresh PBS buffer. The resuspended samples were analyzed under a confocal-optical microscope.

2. Results and Discussion

2.1. Preparation of SL M-SiO_2 NPs and DL M-SiO_2 NPs

To solve the problem of "slow accumulation and low separation yield of single Fe_3O_4 NPs", large numbers of Fe_3O_4 NPs were immobilized onto silica template particles by applying two strategies.

First, surface modification for constructing SiO_2@multi Fe_3O_4 NPs composite structure. To immobilize Fe_3O_4 NPs onto silica surface densely and to prevent detaching the immobilized Fe_3O_4 NPs from it during further silica coating, we modified the surface of SiO_2 NPs with dopamine (dop-SiO_2 NPs), which could form a catecholate-iron complex with Fe_3O_4 NPs. As expected, Fe_3O_4 NPs were densely immobilized onto the dop-SiO_2 NP surface.

Second, loading large numbers of Fe_3O_4 NPs onto silica NPs by forming multilayered structure. With our surface modification method, ~400 units of Fe_3O_4 NPs were immobilized onto the surface of silica core particle. And, additional ~800 units of Fe_3O_4

NPs were loaded onto the surface of SL M-SiO_2 NP.

The fabrication flow for the proposed DL M-SiO_2 NPs is illustrated in Fig. 34. The DL M-SiO_2 NPs had a core-shell structure; multiple Fe_3O_4 NPs were placed on the shell of the silica core as a laminated double-layer structure. The silica NPs were used as the core template for easy handling and reproducible preparation. The Fe_3O_4 NPs immobilized double-layer was designed to increase the loading level of the MNPs on the silica nanostructure to achieve a strong magnetic property. The surface of DL M-SiO_2 NPs was finally covered with a silica layer for biocompatibility and easy functionalization.

The DL M-SiO_2 NPs were fabricated using the following procedure. First, the core silica NPs were prepared using the Stöber method.[123] The silica NPs were spherical with a diameter of ~200 nm. Then, carboxylic group-ended silica NPs (SiO_2-COOH NPs) were prepared using a general surface modification method with APTS[137] and succinic anhydride.[138] A sidrophore-inspired method was adapted to efficiently immobilize Fe_3O_4 NPs on the surface of

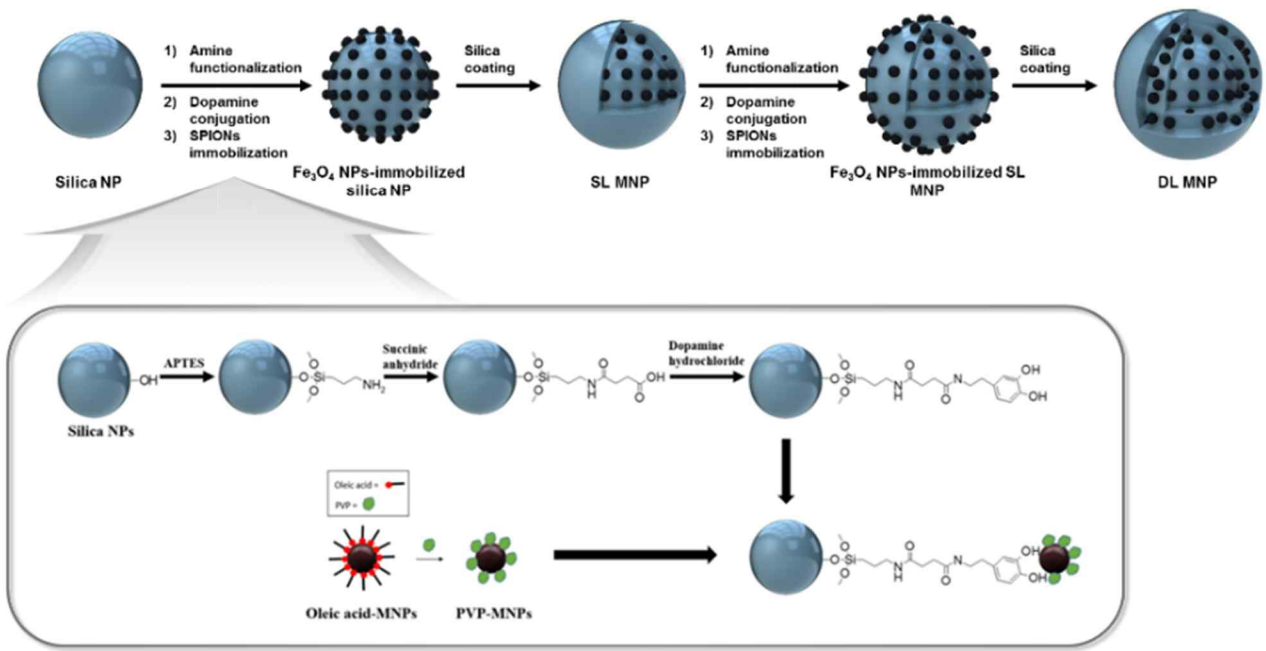

Figure 34. Synthetic scheme for the Fe_3O_4 NPs single-layered silica NPs (SL M-SiO_2 NPs) and Fe_3O_4 NPs double-layered silica NPs (DL M-SiO_2 NPs).[139]

the silica NPs,[140,141] Dopamine was introduced on the surface of the SiO_2-COOH NPs by forming an amide bond. The 18 nm-sized amphiphilic PVP-stabilized Fe_3O_4 NPs (Fig. 26c), which were prepared separately, were immobilized on the dopamine-conjugated SiO_2 NPs (dop-SiO_2 NPs) by forming a catecholate-iron complex. As shown in Fig. 35a, Fe_3O_4 NPs were densely immobilized on the dop-SiO_2 NP surface (~400 Fe_3O_4 NP units/silica core particle). The catecholate-iron complex between the PVP-coated Fe_3O_4 NPs and the dop-SiO_2 NPs maintained their structure even after 1 h of sonication. To identify the phase of exploited Fe_3O_4 NPs before and after ligand exchange, each of oleate-stabilized Fe_3O_4 NPs and the immobilized ones on dopamine-coated SiO_2 NPs were analyzed using high resolution transmission electron microscope (HR-TEM), respectively. The distance between two adjacent planes of oleic acid-stabilized Fe_3O_4 NP is measured to be 4.9 Å (Fig. 36a), corresponding to the typical parameter of (111) plane of the inverse spinel structured Fe_3O_4. The immobilized Fe_3O_4 NPs onto dopamine-coated SiO_2 NPs have a lattice parameter of 2.8 Å, which is well matched with

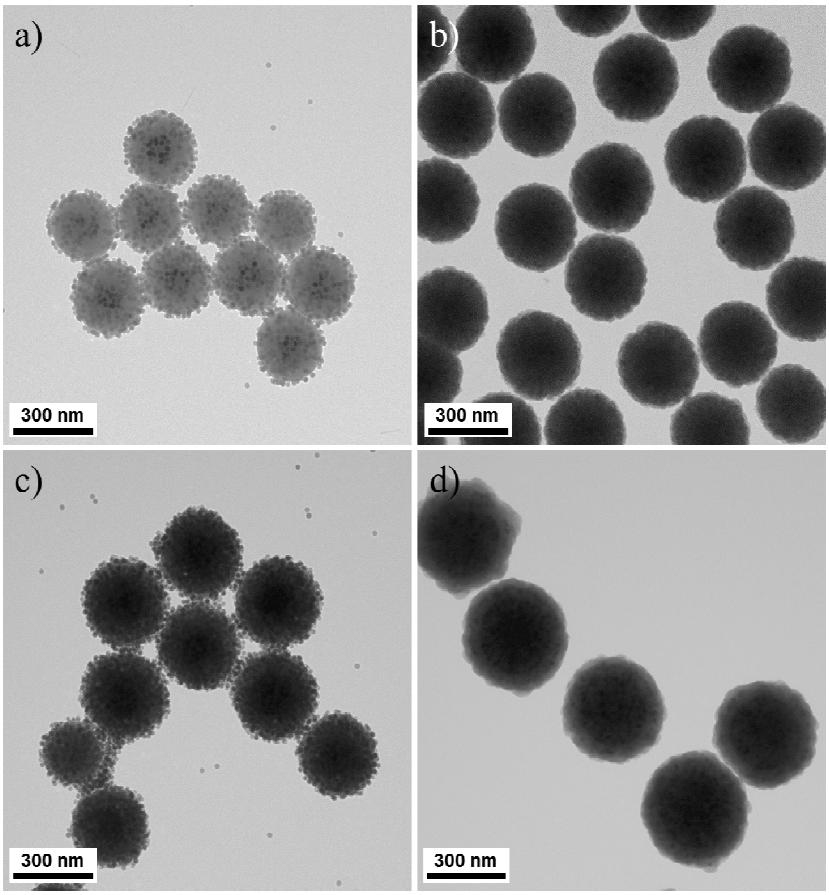

Figure 35. Transmission electron microscopic (TEM) images of the prepared magnetic NPs. Images of a) Fe_3O_4 NPs-immobilized SiO_2 NPs, b) SL M-SiO_2 NPs, c) Fe_3O_4 NPs-immobilized SL M-SiO_2 NPs, and d) DL M-SiO_2 NPs.[139]

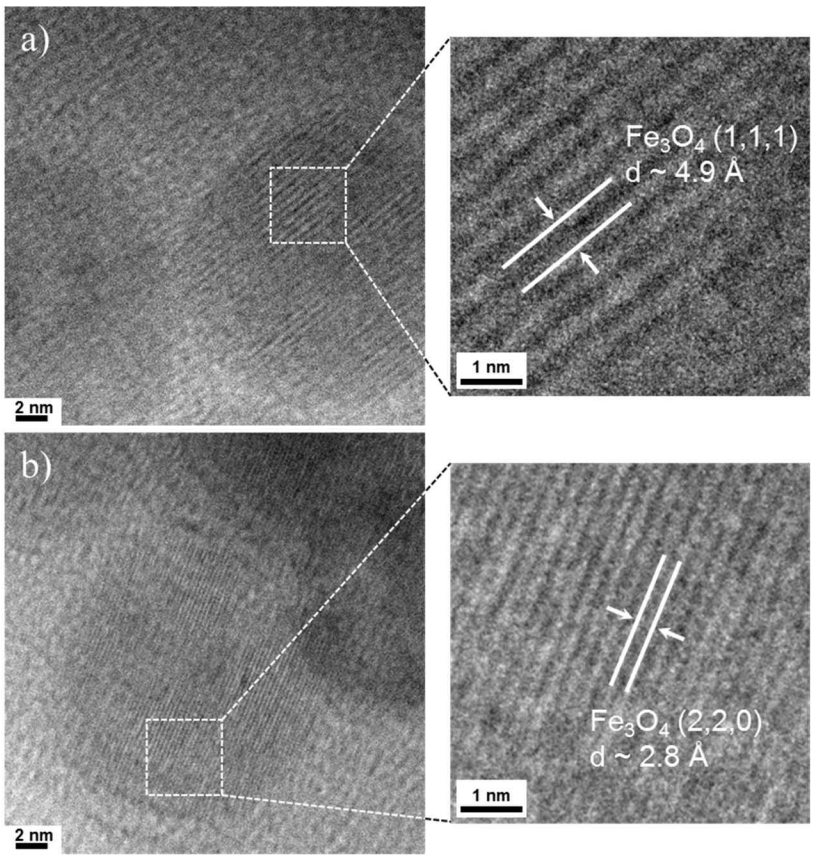

Figure 36. Lattice fringes of Fe_3O_4 NPs before and after the ligand exchange. HR-TEM images of a) oleate-stabilized Fe_3O_4 NPs and b) immobilized Fe_3O_4 NPs onto the surface of dopamine-conjugated SiO_2 NPs. Arrows indicate the distance between two adjacent planes.[139]

(220) plane of Fe_3O_4 (Fig. 36b). These results demonstrate that Fe_3O_4 NPs maintained their structure after the ligand exchange.

TEOS was added to the Fe_3O_4 NPs-immobilized SiO_2 NPs to form the silica shell. The resulting SL M-SiO_2 NPs were encapsulated in a monodispersed manner with a silica shell of ~30 nm thickness, without forming aggregations as shown in Fig. 35b. The remaining PVP moiety on the NP surface may have affected successful silica coating because its amphiphilic character could enhance affinity between Fe_3O_4 NPs and silica.[142] The size of SL M-SiO_2 NPs was ~300 nm, and the number of immobilized Fe_3O_4 NPs remained the same after silica coating. DL M-SiO_2 NPs were prepared by repeating the aforementioned method. As a result, ~800 units of Fe_3O_4 NPs were additionally loaded onto the NPs, as shown Fig. 35c. The two-fold higher Fe_3O_4 NPs loading on SL M-SiO_2 NPs than the bare dop-SiO_2 NPs was the result of an almost two-fold larger surface area.

After introducing additional Fe_3O_4 NP layers and a silica shell (~30 nm), the size of DL M-SiO_2 NPs was increased to ~400 nm, as shown in Fig. 35d. The prepared NPs were uniform in size and

no aggregation of M-SiO_2 NPs was detected. In addition, ~1,200 Fe_3O_4 NP units were successfully packed onto a single silica nanostructure due to the high affinity between the catechol moiety and iron oxide as well as the double-layered structure.

2.2. Magnetic Property Analysis

We investigated the magnetic properties of SL M-SiO_2 NPs and DL M-SiO_2 NPs. There have been enormous amounts of studies on the MNPs-exploited biomolecule separation. Most of the studies have focused on target cell separation, gaining more than 70-90% separation efficiency.[143-145] Even though magnetic strength of the exploited MNPs is low, high separation efficiency could be obtained, if large number of MNPs is attached to a single cell. On the other hand, to obtain high efficiency in separating smaller biomolecules, magnetic strength of a single MNP itself is a critical issue. First, we analyzed the accumulation kinetics of MNPs using an external magnetic field. Samples of SL M-SiO_2 NPs, DL M-SiO_2 NPs, and silica-coated Fe_3O_4 NPs in a 1.5 mL microtube were separated with a NdFeB magnet. The silica-coated Fe_3O_4 NPs (Fig. 22c) were prepared by using our previously reported method.[122] To obtain the accumulation rate of MNPs, the following procedure was followed, as shown in Fig. 37a. First, we measured the concentration of NPs in MNPs-dispersed ethanol solution as the

initial concentration **(C_i)**. The concentration of NPs was analyzed using Nanosight LM10 (Malvern Instrument). Subsequently, we put a NdFeB magnet at a distance of 1 mm from the NPs suspension. At each time intervals after placing the magnet, a small portion of the remnant NPs suspension was removed and its concentration **(C_r)** was measured. The accumulation rate was obtained by subtracting $\mathbf{C_r}$ from $\mathbf{C_i}$. The concentration of MNPs was measured at selected time intervals (1, 2, 3, 5, 10, and 30 min after placing the magnet). As shown in Fig. 37b, DL M-SiO_2 NPs were collected more efficiently than silica-coated Fe_3O_4 NPs or SL M-SiO_2 NPs. Although the SL M-SiO_2 NPs showed a better accumulation profile compared to that of the silica-coated Fe_3O_4 NPs, both NPs gave a saturated plateau before full recovery. The surface charge of the MNPs could cause a charge-charge repulsion, which might lead to incomplete accumulation of NPs. However, all DL M-SiO_2 NPs accumulated quantitatively in 30 min, indicating that DL M-SiO_2 NPs contained a sufficient number of Fe_3O_4 NPs to overcome the repulsive interactions of the silica-coated NPs. In addition, as time elaped, the magnetic accumulation

speed of all types of MNPsbecame slow. This phenomenon is well matched with the previously reported magnetic separation kinetics of single-domain NPs.[146,147] Under external magnetic fields, the single-domain NPs are known to form transient aggregation, which is magnetically more responsive than individual NPs. The separation of single-domain NPs would be mainly driven by this aggregation of NPs rather than individual NP itself. This makes the accumulation rate of single-domain NPs highly dependent on the concentration of NPs. Hence, as $\mathbf{C_r}$ decreases during the magnetic separation, the accumulation rate of MNPs will be slow down.

The field-dependent magnetism of the DL M-SiO_2 NPs at 300 K exhibited superparamagnetic characteristics (Fig. 38), with a saturated magnetization of 5.0 emu/g. Although the magnetization value per weight was lower than 18 nm Fe_3O_4 (60.0 emu/g), each DL M-SiO_2 NP unit had a 500-fold stronger magnetic property than that of bare 18 nm Fe_3O_4. Details of the calculations and assumptions are described in Appendix.

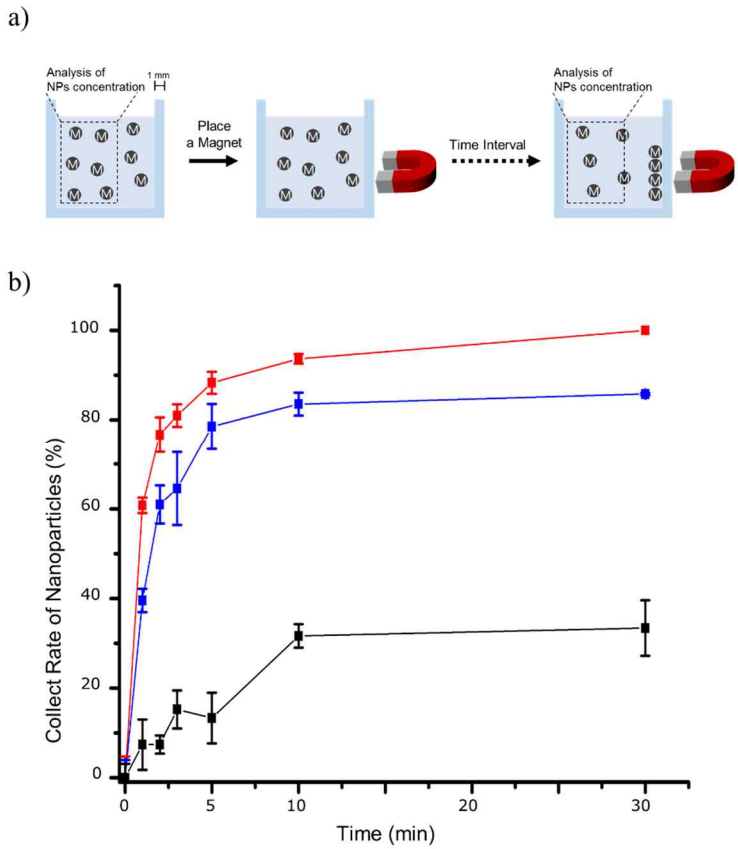

Figure 37. (a) Scheme of analysis for accumulation profiles for the MNPs and (b) accumulation profiles for DL M-SiO_2 NPs (red), SL M-SiO_2 NPs (blue), and silica-coated Fe_3O_4 NPs (black).[139]

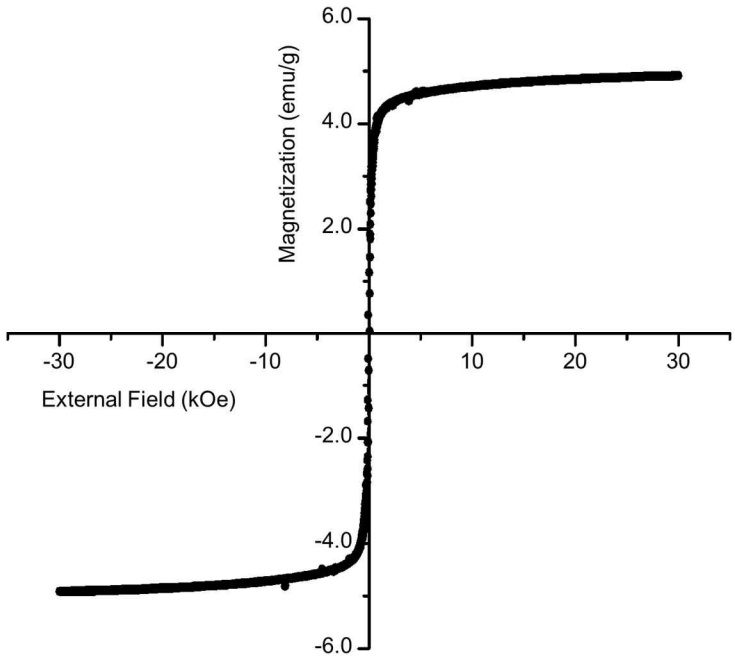

Figure 38. Hysteresis loop of DL M-SiO_2 NPs.[139]

2.3. Stability Analysis

To confirm the stability of the prepared M-SiO_2 NPs, SL M-SiO_2 NP were stored in three kinds of buffer solution of pH 4, 7 and 10 for 7 days, respectively. The SL M-SiO_2 NP maintained their original structure as well as the dispersion property and none of Fe_3O_4 NPs was leached out under acidic (pH 4, Fig. 39a) and neutral condition (pH 7, Fig. 9b). On the other hand, the silica surface layer of SL M-SiO_2 NP was slightly degraded under basic condition (pH 10, Fig. 39c), although Fe_3O_4 NPs leaching was not found. Since most of the silica-based materials are working properly at pH 6~8,[148-151] our M-SiO_2 NPs might be suitable for common bio-application. In addition, these NPs maintained their hydrodynamic size for 7 days in cell culture medium (Fig. 40a), and did not show significant cytotoxic activity, based on CCK-8 assay results (Fig. 40b). These results clearly demonstrate the great potential of DL M-SiO_2 NP for biomolecule separations.

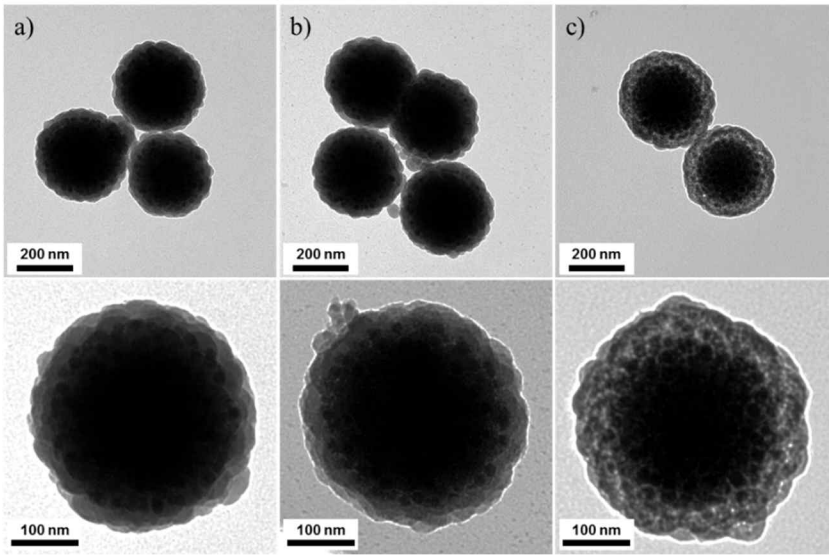

Figure 39. Stability test of SL M-SiO_2 NP under various pH conditions. TEM images of SL M-SiO_2 NP after storage for 7 days at (a, top and bottom) pH 4 potassium hydrogen phthalate buffer, (b, top and bottom) pH 7 potassium hydrogen phosphate buffer, and (c, top and bottom) pH 10 sodium borate buffer, respectively.[139]

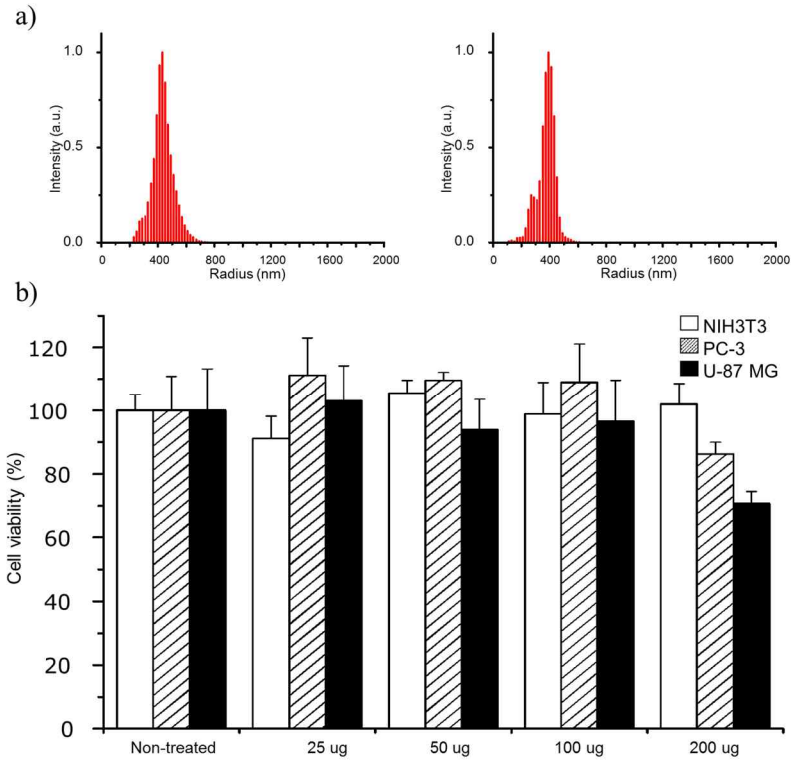

Figure 40. *In vitro* applicability analysis of SL M-SiO_2 NPs. Hydrodynamic radius of SL M-SiO_2 NP after storage for 7 days at (a/left) pH 7 potassium hydrogen phosphate buffer and (a/right) cell culture medium; 10% fetal bovine serum (FBS), 10 U/mL of penicillin, and 10 μg/mL of streptomycin. (b) CCK-8 assay of DL M-SiO_2 NPs. The cell viability data were obtained after subtracting the measured intensity of control group, i.e. DL M-SiO_2 NPs-containing bare medium.[139]

2.4. Magnetic Field-Assisted Protein Separation

Streptavidin was separated to demonstrate that the NPs could be used to separate proteins with a magnet. Biotin-conjugated DL M-SiO_2 NPs and bare DL M-SiO_2 NPs were incubated with FITC-streptavidin in a 1.5 mL microtube. Biotin was conjugated easily to the NPs through a typical amine functionalization onto the silica surface followed by amide coupling. A magnet was placed close to one side of the two sample tubes for 30 min. Thereafter, the streptavidin captured M-SiO_2 NP suspension was removed, and the streptavidin-captured M-SiO_2 NP portion accumulated by the magnet was resuspended in fresh PBS buffer. The resuspended samples were analyzed under a confocal-optical microscope. All biotin-conjugated DL M-SiO_2 NPs observed under the optical microscope illuminated green fluorescence originating from FITC-streptavidin, indicating that streptavidin was clearly separated out using the biotin-conjugated DL M-SiO_2 NPs (Fig. 37a and b). No green fluorescence of FITC-streptavidin was observed from the bare DL M-SiO_2 NPs (Fig. 37c and d).

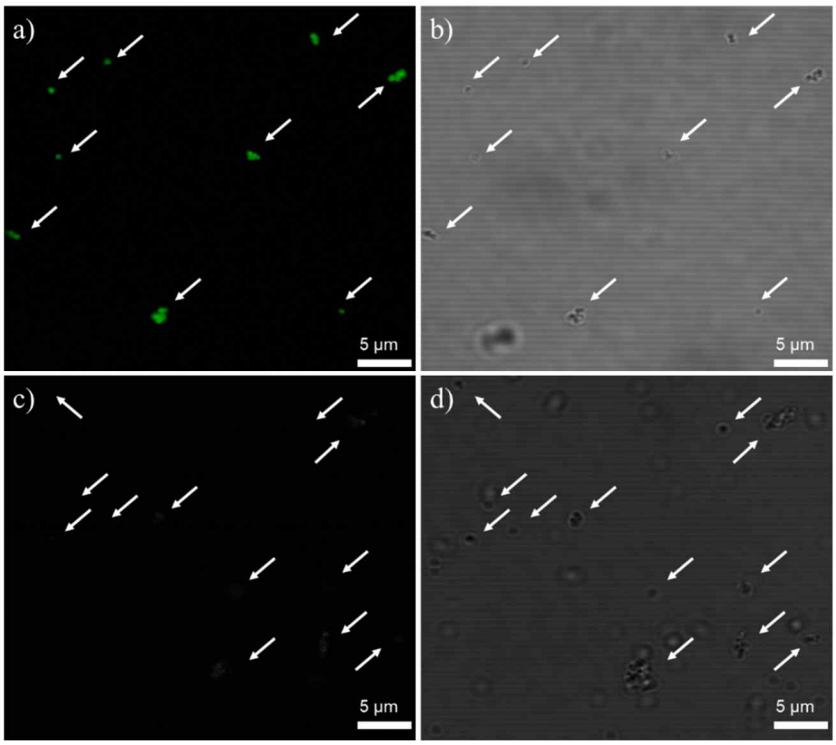

Figure 41. FITC-streptavidin separation using biotin-conjugated DL M-SiO_2 NP. Fluorescence and optical microscopic images of (a, b) biotin-conjugated DL M-SiO_2 NPs and (c, d) bare DL M-SiO_2 NPs after incubation with FITC-streptavidin and magnet-induced separation. Arrows indicate the detected NPs.[139]

3. Conclusion

Core/multi-shell type silica-coated magnetic NPs were synthesized. We utilized the catecholate-iron complex-based surface modification method and fabricated a double-layered structure to immobilize a large number of Fe_3O_4 NPs on silica NPs. As a result, MNPs-embedded silica NPs, which contain 1,200 units of Fe_3O_4 NPs, were successfully prepared. The resulting NPs were highly uniform in size, and exhibited a superparamagnetic property. They were quantitatively collected using a magnet in a short period of time. Moreover, FITC-streptavidin was effectively separated by biotin-conjugated DL M-SiO_2 NPs using an external magnetic field, showing that the DL M-SiO_2 NPs have great potential to be exploited for biomolecule separation.

References

1. Rossetti R, Beck SM, Brus LE (1983) Resonance Raman Investigation of the Pi-Star Antibonding Distribution in Excited Triplet Aqueous Para-Benzoquinone. Journal of Physical Chemistry 87: 3058-3061.

2. Alivisatos AP (1996) Perspectives on the physical chemistry of semiconductor nanocrystals. Journal of Physical Chemistry 100: 13226-13239.

3. Ekimov AI, Efros AL, Onushchenko AA (1985) Quantum Size Effect in Semiconductor Microcrystals. Solid State Communications 56: 921-924.

4. Smith AM, Nie SM (2004) Chemical analysis and cellular imaging with quantum dots. Analyst 129: 672-677.

5. Boatman EM, Lisensky GC, Nordell KJ (2005) A safer, easier, faster synthesis for CdSe quantum dot nanocrystals. Journal of Chemical Education 82: 1697-1699.

6. Wei SH, Zunger A (1998) Calculated natural band offsets of all II-VI and Ill-V semiconductors: Chemical trends and the role of cation d orbitals. Applied Physics Letters 72: 2011-2013.

7. Zhong XH, Han MY, Dong ZL, White TJ, Knoll W (2003) Composition-tunable ZnxCd1-xSe nanocrystals with high luminescence and stability. Journal of the American Chemical Society 125: 8589-8594.

8. Zhong XH, Feng YY, Knoll W, Han MY (2003) Alloyed ZnxCd1-xS nanocrystals with highly narrow luminescence spectral width. Journal of the American Chemical Society 125: 13559-13563.

9. Bailey RE, Nie SM (2003) Alloyed semiconductor quantum dots: Tuning the optical properties without changing the particle size. Journal of the American Chemical Society 125: 7100-7106.

10. Kim S, Fisher B, Eisler HJ, Bawendi M (2003) Type-II quantum dots: CdTe/CdSe(core/shell) and CdSe/ZinTe(core/shell) heterostructures. Journal of the American Chemical Society 125: 11466-11467.

11. Wehrenberg BL, Wang CJ, Guyot-Sionnest P (2002) Interband and intraband optical studies of PbSe colloidal quantum dots. Journal of Physical Chemistry B 106: 10634-10640.

12. Rosenthal SJ (2001) Bar-coding biomolecules with fluorescent nanocrystals. Nature Biotechnology 19: 621-622.

13. Murray CB, Norris DJ, Bawendi MG (1993) Synthesis and Characterization of Nearly Monodisperse Cde (E = S, Se, Te) Semiconductor Nanocrystallites. Journal of the American Chemical Society 115: 8706-8715.

14. Wu XY, Liu HJ, Liu JQ, Haley KN, Treadway JA, Larson JP, Ge NF, Peale F, Bruchez MP (2003) Immunofluorescent labeling of cancer marker Her2 and other cellular targets with semiconductor quantum dots (vol 21, pg 41, 2003). Nature Biotechnology 21: 452-452.

15. Gao XH, Yang LL, Petros JA, Marshal FF, Simons JW, Nie SM (2005) In vivo molecular and cellular imaging with quantum dots. Current Opinion in Biotechnology 16: 63-72.

16. Chan WCW, Nie SM (1998) Quantum dot bioconjugates for ultrasensitive nonisotopic detection. Science 281: 2016-2018.

17. Bruchez M, Moronne M, Gin P, Weiss S, Alivisatos AP (1998) Semiconductor nanocrystals as fluorescent biological labels. Science 281: 2013-2016.

18. Kamat PV (2008) Quantum Dot Solar Cells. Semiconductor Nanocrystals as Light Harvesters. Journal of Physical Chemistry C 112: 18737-18753.

19. Robel I, Subramanian V, Kuno M, Kamat PV (2006) Quantum dot solar cells. Harvesting light energy with CdSe nanocrystals molecularly linked to mesoscopic TiO_2 films. Journal of the American Chemical Society 128: 2385-2393.

20. Nozik AJ (2002) Quantum dot solar cells. Physica E-Low-Dimensional Systems & Nanostructures 14: 115-120.

21. Tang J, Kemp KW, Hoogland S, Jeong KS, Liu H, Levina L, Furukawa M, Wang XH, Debnath R, Cha DK, Chou KW, Fischer A, Amassian A, Asbury JB, Sargent EH (2011) Colloidal-quantum-dot photovoltaics using atomic-ligand passivation. Nature Materials 10: 765-771.

22. Rho WY, Choi JW, Lee HY, Kyeong S, Lee SH, Jung HS, Jung S, Sung YE, Lee YS, Jun BH (2014) Dye-sensitized solar cells with

silica-coated quantum dot-embedded nanoparticles used as a light-harvesting layer. New Journal of Chemistry 38: 910-913.

23. Johnston KW, Pattantyus-Abraham AG, Clifford JP, Myrskog SH, MacNeil DD, Levina L, Sargent EH (2008) Schottky-quantum dot photovoltaics for efficient infrared power conversion. Applied Physics Letters 92.

24. Schierhorn M, Boettcher SW, Peet JH, Matioli E, Bazan GC, Stucky GD, Moskovits M (2010) CdSe Nanorods Dominate Photocurrent of Hybrid CdSe-P3HT Photovoltaic Cell. Acs Nano 4: 6132-6136.

25. Colvin VL, Schlamp MC, Alivisatos AP (1994) Light-Emitting-Diodes Made from Cadmium Selenide Nanocrystals and a Semiconducting Polymer. Nature 370: 354-357.

26. Li YQ, Rizzo A, Cingolani R, Gigli G (2006) Bright white-light-emitting device from ternary nanocrystal composites. Advanced Materials 18: 2545-2548.

27. Rizzo A, Mazzeo M, Biasiucci M, Cingolani R, Gigli G (2008) White Electroluminescence from a Microcontact-Printing-Deposited CdSe/ZnS Colloidal Quantum-Dot Monolayer. Small 4: 2143-2147.

28. Gao MY, Richter B, Kirstein S (1997) White-light electroluminescence from a self-assembled Q-CdSe/PPV multilayer structures. Advanced Materials 9: 802-805.

29. Ali M, Chattopadhyay S, Nag A, Kumar A, Sapra S, Chakraborty S,

Sarma DD (2007) White-light emission from a blend of CdSeS nanocrystals of different Se : S ratio. Nanotechnology 18.

30. Chen HS, Wang SJJ, Lo CJ, Chi JY (2005) White-light emission from organics-capped ZnSe quantum dots and application in white-light-emitting diodes. Applied Physics Letters 86.

31. Coe S, Woo WK, Bawendi M, Bulovic V (2002) Electroluminescence from single monolayers of nanocrystals in molecular organic devices. Nature 420: 800-803.

32. Zhuang L, Guo LJ, Chou SY (1998) Silicon single-electron quantum-dot transistor switch operating at room temperature. Applied Physics Letters 72: 1205-1207.

33. Leobandung E, Guo LJ, Chou SY (1995) Single Hole Quantum-Dot Transistors in Silicon. Applied Physics Letters 67: 2338-2340.

34. Konstantatos G, Badioli M, Gaudreau L, Osmond J, Bernechea M, de Arquer FPG, Gatti F, Koppens FHL (2012) Hybrid graphene-quantum dot phototransistors with ultrahigh gain. Nature Nanotechnology 7: 363-368.

35. Gao XH, Cui YY, Levenson RM, Chung LWK, Nie SM (2004) In vivo cancer targeting and imaging with semiconductor quantum dots. Nature Biotechnology 22: 969-976.

36. Wang SP, Mamedova N, Kotov NA, Chen W, Studer J (2002) Antigen/antibody immunocomplex from CdTe nanoparticle bioconjugates. Nano Letters 2: 817-822.

37. Goldman ER, Medintz IL, Whitley JL, Hayhurst A, Clapp AR,

Uyeda HT, Deschamps JR, Lassman ME, Mattoussi H (2005) A hybrid quantum dot-antibody fragment fluorescence resonance energy transfer-based TNT sensor. Journal of the American Chemical Society 127: 6744-6751.

38. Zhang CY, Yeh HC, Kuroki MT, Wang TH (2005) Single-quantum-dot-based DNA nanosensor. Nature Materials 4: 826-831.

39. So MK, Xu CJ, Loening AM, Gambhir SS, Rao JH (2006) Self-illuminating quantum dot conjugates for in vivo imaging. Nature Biotechnology 24: 339-343.

40. Willner I, Patolsky F, Wasserman J (2001) Photoelectrochemistry with controlled DNA-cross-linked CdS nanoparticle arrays. Angewandte Chemie-International Edition 40: 1861-1864.

41. Katz E, Zayats M, Willner I, Lisdat F (2006) Controlling the direction of photocurrents by means of CdS nanoparticles and cytochrome c-mediated biocatalytic cascades. Chemical Communications: 1395-1397.

42. Gill R, Zayats M, Willner I (2008) Semiconductor quantum dots for bioanalysis. Angewandte Chemie-International Edition 47: 7602-7625.

43. Medintz IL, Uyeda HT, Goldman ER, Mattoussi H (2005) Quantum dot bioconjugates for imaging, labelling and sensing. Nature Materials 4: 435-446.

44. Qu LH, Peng XG (2002) Control of photoluminescence properties of CdSe nanocrystals in growth. Journal of the American

Chemical Society 124: 2049-2055.

45. Cordero SR, Carson PJ, Estabrook RA, Strouse GF, Buratto SK (2000) Photo-activated luminescence of CdSe quantum dot monolayers. Journal of Physical Chemistry B 104: 12137-12142.

46. Gerion D, Pinaud F, Williams SC, Parak WJ, Zanchet D, Weiss S, Alivisatos AP (2001) Synthesis and properties of biocompatible water-soluble silica-coated CdSe/ZnS semiconductor quantum dots. Journal of Physical Chemistry B 105: 8861-8871.

47. Pellegrino T, Manna L, Kudera S, Liedl T, Koktysh D, Rogach AL, Keller S, Radler J, Natile G, Parak WJ (2004) Hydrophobic nanocrystals coated with an amphiphilic polymer shell: A general route to water soluble nanocrystals. Nano Letters 4: 703-707.

48. Smith AM, Duan HW, Rhyner MN, Ruan G, Nie SM (2006) A systematic examination of surface coatings on the optical and chemical properties of semiconductor quantum dots. Physical Chemistry Chemical Physics 8: 3895-3903.

49. Pellegrino T, Kudera S, Liedl T, Javier AM, Manna L, Parak WJ (2005) On the development of colloidal nanoparticles towards multifunctional structures and their possible use for biological applications. Small 1: 48-63.

50. Baumle M, Stamou D, Segura JM, Hovius R, Vogel H (2004) Highly fluorescent streptavidin-coated CdSe nanoparticles: Preparation in water, characterization, and micropatterning. Langmuir 20: 3828-3831.

51. Evanoff DD, Hayes SE, Ying Y, Shim GH, Lawrence JR, Carroll JB, Roeder RD, Houchins JM, Huebner CE, Foulger SH (2007) Functionalization of crystalline colloidal arrays through click chemistry. Advanced Materials 19: 3507-3512.

52. Willard DM, Carillo LL, Jung J, Van Orden A (2001) CdSe-ZnS quantum dots as resonance energy transfer donors in a model protein-protein binding assay. Nano Letters 1: 469-474.

53. Medintz IL, Clapp AR, Mattoussi H, Goldman ER, Fisher B, Mauro JM (2003) Self-assembled nanoscale biosensors based on quantum dot FRET donors. Nature Materials 2: 630-638.

54. Uyeda HT, Medintz IL, Jaiswal JK, Simon SM, Mattoussi H (2005) Synthesis of compact multidentate ligands to prepare stable hydrophilic quantum dot fluorophores. Journal of the American Chemical Society 127: 3870-3878.

55. Liu W, Howarth M, Greytak AB, Zheng Y, Nocera DG, Ting AY, Bawendi MG (2008) Compact biocompatible quantum dots functionalized for cellular imaging. Journal of the American Chemical Society 130: 1274-1284.

56. Bitar A, Ahmad NM, Fessi H, Elaissari A (2012) Silica-based nanoparticles for biomedical applications. Drug Discovery Today 17: 1147-1154.

57. Halas NJ (2008) Nanoscience under glass: The versatile chemistry of silica nanostructures. Acs Nano 2: 179-183.

58. Altinoglu EI, Adair JH (2010) Near infrared imaging with

nanoparticles. Wiley Interdisciplinary Reviews-Nanomedicine and Nanobiotechnology 2: 461-477.

59. Koto M, Marshall AF, Goldthorpe IA, McIntyre PC (2010) Gold-Catalyzed Vapor-Liquid-Solid Germanium-Nanowire Nucleation on Porous Silicon. Small 6: 1032-1037.

60. Kim J, Lee JE, Lee J, Yu JH, Kim BC, An K, Hwang Y, Shin CH, Park JG, Kim J, Hyeon T (2006) Magnetic fluorescent delivery vehicle using uniform mesoporous silica spheres embedded with monodisperse magnetic and semiconductor nanocrystals. Journal of the American Chemical Society 128: 688-689.

61. Park W, Kim MJ, Choe Y, Kim SK, Woo K (2014) Highly photoluminescent superparamagnetic silica composites for on-site biosensors. Journal of Materials Chemistry B 2: 1938-1944.

62. Zheng J, Feng WJ, Cheng GF, Huang CH, Lin L, He PG, Fang YZ (2007) Approaching signal amplification of electrochemical biosensor for thrombin based on enrichment of gold nanoparticles through hybridization with complementary oligonucleotide. Chemical Journal of Chinese Universities-Chinese 28: 2274-2279.

63. Yi DK, Selvan ST, Lee SS, Papaefthymiou GC, Kundaliya D, Ying JY (2005) Silica-coated nanocomposites of magnetic nanoparticles and quantum dots. Journal of the American Chemical Society 127: 4990-4991.

64. Pillai PP, Reisewitz S, Schroeder H, Niemeyer CM (2010) Quantum-Dot-Encoded Silica Nanospheres for Nucleic Acid Hybridization. Small 6: 2130-2134.

65. Behrendt JM, Afzaal M, Alexander LM, Bradley M, Hine AV, Nagel D, O'Brien P, Presland K, Sutherland AJ (2009) Thiol-containing microspheres as polymeric ligands for the immobilisation of quantum dots. Journal of Materials Chemistry 19: 215-221.

66. Lu ZD, Gao CB, Zhang Q, Chi MF, Howe JY, Yin YD (2011) Direct Assembly of Hydrophobic Nanoparticles to Multifunctional Structures. Nano Letters 11: 3404-3412.

67. Choi HS, Liu WH, Liu FB, Nasr K, Misra P, Bawendi MG, Frangioni JV (2010) Design considerations for tumour-targeted nanoparticles. Nature Nanotechnology 5: 42-47.

68. Cho M, Lim K, Woo K (2010) Facile synthesis and optical properties of colloidal silica microspheres encapsulating a quantum dot layer. Chemical Communications 46: 5584-5586.

69. Lu AH, Salabas EL, Schuth F (2007) Magnetic nanoparticles: Synthesis, protection, functionalization, and application. Angewandte Chemie-International Edition 46: 1222-1244.

70. Jeong U, Teng XW, Wang Y, Yang H, Xia YN (2007) Superparamagnetic colloids: Controlled synthesis and niche applications. Advanced Materials 19: 33-60.

71. Sun C, Lee JSH, Zhang MQ (2008) Magnetic nanoparticles in MR imaging and drug delivery. Advanced Drug Delivery Reviews 60: 1252-1265.

72. Teja AS, Koh PY (2009) Synthesis, properties, and applications of magnetic iron oxide nanoparticles. Progress in Crystal Growth and

Characterization of Materials 55: 22-45.

73. Pankhurst QA, Thanh NTK, Jones SK, Dobson J (2009) Progress in applications of magnetic nanoparticles in biomedicine. Journal of Physics D-Applied Physics 42.

74. Tadic M, Kralj S, Jagodic M, Hanzel D, Makovec D (2014) Magnetic properties of novel superparamagnetic iron oxide nanoclusters and their peculiarity under annealing treatment. Applied Surface Science 322: 255-264.

75. Xu CJ, Xu KM, Gu HW, Zhong XF, Guo ZH, Zheng RK, Zhang XX, Xu B (2004) Nitrilotriacetic acid-modified magnetic nanoparticles as a general agent to bind histidine-tagged proteins. Journal of the American Chemical Society 126: 3392-3393.

76. Bucak S, Jones DA, Laibinis PE, Hatton TA (2003) Protein separations using colloidal magnetic nanoparticles. Biotechnology Progress 19: 477-484.

77. Sonti SV, Bose A (1995) Cell-Separation Using Protein-a-Coated Magnetic Nanoclusters. Journal of Colloid and Interface Science 170: 575-585.

78. Neveu S, Bee A, Robineau M, Talbot D (2002) Size-selective chemical synthesis of tartrate stabilized cobalt ferrite ionic magnetic fluid. Journal of Colloid and Interface Science 255: 293-298.

79. Grasset F, Labhsetwar N, Li D, Park DC, Saito N, Haneda H, Cador O, Roisnel T, Mornet S, Duguet E, Portier J, Etourneau J (2002)

Synthesis and magnetic characterization of zinc ferrite nanoparticles with different environments: Powder, colloidal solution, and zinc ferrite-silica core-shell nanoparticles. Langmuir 18: 8209-8216.

80. Sun SH, Zeng H (2002) Size-controlled synthesis of magnetite nanoparticles. Journal of the American Chemical Society 124: 8204-8205.

81. Park SJ, Kim S, Lee S, Khim ZG, Char K, Hyeon T (2000) Synthesis and magnetic studies of uniform iron nanorods and nanospheres. Journal of the American Chemical Society 122: 8581-8582.

82. Puntes VF, Krishnan KM, Alivisatos AP (2001) Colloidal nanocrystal shape and size control: The case of cobalt. Science 291: 2115-2117.

83. Chen Q, Rondinone AJ, Chakoumakos BC, Zhang ZJ (1999) Synthesis of superparamagnetic MgFe2O4 nanoparticles by coprecipitation. Journal of Magnetism and Magnetic Materials 194: 1-7.

84. Park J, An KJ, Hwang YS, Park JG, Noh HJ, Kim JY, Park JH, Hwang NM, Hyeon T (2004) Ultra-large-scale syntheses of monodisperse nanocrystals. Nature Materials 3: 891-895.

85. Sun SH, Murray CB, Weller D, Folks L, Moser A (2000) Monodisperse FePt nanoparticles and ferromagnetic FePt nanocrystal superlattices. Science 287: 1989-1992.

86. Shevchenko EV, Talapin DV, Rogach AL, Kornowski A, Haase M, Weller H (2002) Colloidal synthesis and self-assembly of COPt3 nanocrystals (vol 124, pg 11480, 2002). Journal of the American Chemical Society 124: 13958-13958.

87. Tartaj P, Morales MD, Veintemillas-Verdaguer S, Gonzalez-Carreno T, Serna CJ (2003) The preparation of magnetic nanoparticles for applications in biomedicine. Journal of Physics D-Applied Physics 36: R182-R197.

88. Bourgeat-Lami E, Lang J (1998) Encapsulation of inorganic particles by dispersion polymerization in polar media - 1. Silica nanoparticles encapsulated by polystyrene. Journal of Colloid and Interface Science 197: 293-308.

89. Gupta AK, Gupta M (2005) Synthesis and surface engineering of iron oxide nanoparticles for biomedical applications. Biomaterials 26: 3995-4021.

90. Vollmer C, Janiak C (2011) Naked metal nanoparticles from metal carbonyls in ionic liquids: Easy synthesis and stabilization. Coordination Chemistry Reviews 255: 2039-2057.

91. Lalatonne Y, Richardi J, Pileni MP (2004) Van der Waals versus dipolar forces controlling mesoscopic organizations of magnetic nanocrystals. Nature Materials 3: 121-125.

92. Mahmoudi M, Sant S, Wang B, Laurent S, Sen T (2011) Superparamagnetic iron oxide nanoparticles (SPIONs): Development, surface modification and applications in chemotherapy. Advanced Drug Delivery Reviews 63: 24-46.

93. Stoeva SI, Huo FW, Lee JS, Mirkin CA (2005) Three-layer composite magnetic nanoparticle probes for DNA. Journal of the American Chemical Society 127: 15362-15363.

94. Tartaj P, Gonzalez-Carreno T, Serna CJ (2001) Single-step nanoengineering of silica coated maghemite hollow spheres with tunable magnetic properties. Advanced Materials 13: 1620-1624.

95. Sailor MJ, Park JH (2012) Hybrid Nanoparticles for Detection and Treatment of Cancer. Advanced Materials 24: 3779-3802.

96. Zhang PH, Cao JT, Min QH, Zhu JJ (2013) Multi-Shell Structured Fluorescent-Magnetic Nanoprobe for Target Cell Imaging and On-Chip Sorting. Acs Applied Materials & Interfaces 5: 7417-7424.

97. Wang LA, Neoh KG, Kang ET, Shuter B (2011) Multifunctional polyglycerol-grafted Fe3O4@SiO2 nanoparticles for targeting ovarian cancer cells. Biomaterials 32: 2166-2173.

98. Yi PW, Chen GC, Zhang HL, Tian F, Tan B, Dai JW, Wang QB, Deng ZW (2013) Magnetic resonance imaging of Fe3O4@SiO2-labeled human mesenchymal stem cells in mice at 11.7 T. Biomaterials 34: 3010-3019.

99. Jun BH, Kim G, Baek J, Kang H, Kim T, Hyeon T, Jeong DH, Lee YS (2011) Magnetic field induced aggregation of nanoparticles for sensitive molecular detection. Physical Chemistry Chemical Physics 13: 7298-7303.

100. Huang CK, Hou CH, Chen CC, Tsai YL, Chang LM, Wei HS, Hsieh KH, Chan CH (2008) Magnetic SiO2/Fe3O4 colloidal

crystals. Nanotechnology 19.

101. Tan XJ, Lu LJ, Wang LZ, Zhang JL (2015) Facile Synthesis of Bimodal Mesoporous Fe3O4@SiO2 Composite for Efficient Removal of Methylene Blue. European Journal of Inorganic Chemistry: 2928-2933.

102. Jun BH, Noh MS, Kim J, Kim G, Kang H, Kim MS, Seo YT, Baek J, Kim JH, Park J, Kim S, Kim YK, Hyeon T, Cho MH, Jeong DH, Lee YS (2010) Multifunctional Silver-Embedded Magnetic Nanoparticles as SERS Nanoprobes and Their Applications. Small 6: 119-125.

103. Kim J, Park S, Lee JE, Jin SM, Lee JH, Lee IS, Yang I, Kim JS, Kim SK, Cho MH, Hyeon T (2006) Designed fabrication of multifunctional magnetic gold nanoshells and their application to magnetic resonance imaging and photothermal therapy. Angewandte Chemie-International Edition 45: 7754-7758.

104. Mi Y, Li K, Liu Y, Pu KY, Liu B, Feng SS (2011) Herceptin functionalized polyhedral oligomeric silsesquioxane - conjugated oligomers - silica/iron oxide nanoparticles for tumor cell sorting and detection. Biomaterials 32: 8226-8233.

105. Wu W, Caruntu D, Martin A, Yu MH, O'Connor CJ, Zhou WL, Chen JF (2007) Synthesis of magnetic hollow silica using polystyrene bead as a template. Journal of Magnetism and Magnetic Materials 311: 578-582.

106. Rose M, Korenblit Y, Kockrick E, Borchardt L, Oschatz M, Kaskel S, Yushin G (2011) Hierarchical Micro- and Mesoporous Carbide-

Derived Carbon as a High-Performance Electrode Material in Supercapacitors. Small 7: 1108-1117.

107. Jun BH, Hwang DW, Jung HS, Jang J, Kim H, Kang H, Kang T, Kyeong S, Lee H, Jeong DH, Kang KW, Youn H, Lee DS, Lee YS (2012) Ultrasensitive, Biocompatible, Quantum-Dot-Embedded Silica Nanoparticles for Bioimaging. Advanced Functional Materials 22: 1843-1849.

108. Graf C, Dembski S, Hofmann A, Ruhl E (2006) A general method for the controlled embedding of nanoparticles in silica colloids. Langmuir 22: 5604-5610.

109. Wang ZB, Guo W, Li L, Luk'yanchuk B, Khan A, Liu Z, Chen ZC, Hong MH (2011) Optical virtual imaging at 50 nm lateral resolution with a white-light nanoscope. Nature Communications 2.

110. Kyeong S, Kang H, Yim J, Jeon SJ, Jeong CH, Lee YS, Jun BH, Kim JH (2013) Quantum dot-assembled nanoparticles with polydiacetylene supramolecule toward label-free, multiplexed optical detection. Journal of Colloid and Interface Science 394: 44-48.

111. Baughman RH, Chance RR (1976) Comments on Optical-Properties of Fully Conjugated Polymers - Analogy between Polyenes and Polydiacetylenes. Journal of Polymer Science Part B-Polymer Physics 14: 2037-2045.

112. Charych DH (1993) Direct Colorimetric Detection of a Receptor-Ligand Interaction by a Polymerized Bilayer Assembly (Vol 261,

Pg 585, 1993). Science 261: 1375-1375.

113. Sun AW, Lauher JW, Goroff NS (2006) Preparation of poly(diiododiacetylene), an ordered conjugated polymer of carbon and iodine. Science 312: 1030-1034.

114. Reppy MA, Pindzola BA (2007) Biosensing with polydiacetylene materials: structures, optical properties and applications. Chemical Communications: 4317-4338.

115. Jun BH, Baek J, Kang H, Park YJ, Jeong DH, Lee YS (2011) Preparation of polydiacetylene immobilized optically encoded beads. Journal of Colloid and Interface Science 355: 29-34.

116. Charych DH, Nagy JO, Spevak W, Bednarski MD (1993) Direct Colorimetric Detection of a Receptor-Ligand Interaction by a Polymerized Bilayer Assembly. Science 261: 585-588.

117. Rangin M, Basu A (2004) Lipopolysaccharide identification with functionalized polydiacetylene liposome sensors. Journal of the American Chemical Society 126: 5038-5039.

118. Song J, Cisar JS, Bertozzi CR (2004) Functional self-assembling bolaamphiphilic polydiacetylenes as colorimetric sensor scaffolds. Journal of the American Chemical Society 126: 8459-8465.

119. Abbasi AZ, Amin F, Niebling T, Friede S, Ochs M, Carregal-Romero S, Montenegro JM, Gil PR, Heimbrodt W, Parak WJ (2011) How Colloidal Nanoparticles Could Facilitate Multiplexed Measurements of Different Analytes with Analyte-Sensitive Organic Fluorophores. Acs Nano 5: 21-25.

120. Nagl S, Wolfbeis OS (2007) Optical multiple chemical sensing: status and current challenges. Analyst 132: 507-511.

121. Olmsted J, Strand M (1983) Fluorescence of Polymerized Diacetylene Bilayer Films. Journal of Physical Chemistry 87: 4790-4792.

122. Rho WY, Kim HM, Kyeong S, Kang YL, Kim DH, Kang H, Jeong C, Kim DE, Lee YS, Jun BH (2014) Facile synthesis of monodispersed silica-coated magnetic nanoparticles. Journal of Industrial and Engineering Chemistry 20: 2646-2649.

123. Stober W, Fink A, Bohn E (1968) Controlled Growth of Monodisperse Silica Spheres in Micron Size Range. Journal of Colloid and Interface Science 26: 62-69.

124. Kyeong S, Jeong C, Kim HY, Hwang DW, Kang H, Yang JK, Lee DS, Bong-Hyun JE, Lee YS (2015) Fabrication of mono-dispersed silica-coated quantum dot-assembled magnetic nanoparticles. Rsc Advances 5: 32072-32077.

125. Liu G, Rodriguez JA, Chang Z, Hrbek J, Gonzalez L (2002) Adsorption of methanethiol on stoichiometric and defective TiO2(110) surfaces: A combined experimental and theoretical study. Journal of Physical Chemistry B 106: 9883-9891.

126. Lim H, Carraro C, Maboudian R, Pruessner MW, Ghodssi R (2004) Chemical and thermal stability of alkanethiol and sulfur passivated InP(100). Langmuir 20: 743-747.

127. Hirai T, Saito T, Komasawa I (2000) Recovery and immobilization

of metal sulfide nanoparticles from reverse micellar system onto thiol-modified polystyrene particles. Journal of Physical Chemistry B 104: 11639-11643.

128. Sathe TR, Agrawal A, Nie SM (2006) Mesoporous silica beads embedded with semiconductor quantum dots and iron oxide nanocrystals: Dual-function microcarriers for optical encoding and magnetic separation. Analytical Chemistry 78: 5627-5632.

129. Jang ES, Lee SY, Cha EJ, Sun IC, Kwon IC, Kim D, Kim YI, Kim K, Ahn CH (2014) Fluorescent Dye Labeled Iron Oxide/Silica Core/Shell Nanoparticle as a Multimodal Imaging Probe. Pharmaceutical Research 31: 3371-3378.

130. Forster T (1948) *Zwischenmolekulare Energiewanderung Und Fluoreszenz. Annalen Der Physik 2: 55-75.

131. Hofig H, Gabba M, Poblete S, Kempe D, Fitter J (2014) Inter-Dye Distance Distributions Studied by a Combination of Single-Molecule FRET-Filtered Lifetime Measurements and a Weighted Accessible Volume (wAV) Algorithm. Molecules 19: 19269-19291.

132. Nigam S, Barick KC, Bahadur D (2011) Development of citrate-stabilized Fe3O4 nanoparticles: Conjugation and release of doxorubicin for therapeutic applications. Journal of Magnetism and Magnetic Materials 323: 237-243.

133. Yu CJ, Wu SM, Tseng WL (2013) Magnetite Nanoparticle-Induced Fluorescence Quenching of Adenosine Triphosphate-BODIPY Conjugates: Application to Adenosine Triphosphate and

Pyrophosphate Sensing. Analytical Chemistry 85: 8559-8565.

134. Sapsford KE, Berti L, Medintz IL (2006) Materials for fluorescence resonance energy transfer analysis: Beyond traditional donor-acceptor combinations. Angewandte Chemie-International Edition 45: 4562-4588.

135. Clapp AR, Medintz IL, Mattoussi H (2006) Forster resonance energy transfer investigations using quantum-dot fluorophores. Chemphyschem 7: 47-57.

136. Kagan CR, Murray CB, Bawendi MG (1996) Long-range resonance transfer of electronic excitations in close-packed CdSe quantum-dot solids. Physical Review B 54: 8633-8643.

137. Hermanson GT (2008) Chapter 2 - The Chemistry of Reactive Groups. In: Hermanson GT, editor. Bioconjugate Techniques (Second Edition). New York: Academic Press. pp. 169-212.

138. Hermanson GT (2008) Chapter 1 - Functional Targets. In: Hermanson GT, editor. Bioconjugate Techniques (Second Edition). New York: Academic Press. pp. 1-168.

139. Kyeong S, Jeong C, Kang H, Cho HJ, Park SJ, Yang JK, Kim S, Kim HM, Jun BH, Lee YS (2015) Double-Layer Magnetic Nanoparticle-Embedded Silica Particles for Efficient Bio-Separation. Plos One 10: e0143727.

140. Jia L, Pei XW, Zhou F, Liu WM (2014) Unconventional Assembly of Bimetallic Au-Ni Janus Nanoparticles on Chemically Modified Silica Spheres. Chemistry-a European Journal 20: 2065-2070.

141. Amstad E, Gillich T, Bilecka I, Textor M, Reimhult E (2009) Ultrastable Iron Oxide Nanoparticle Colloidal Suspensions Using Dispersants with Catechol-Derived Anchor Groups. Nano Letters 9: 4042-4048.

142. Graf C, Vossen DLJ, Imhof A, van Blaaderen A (2003) A general method to coat colloidal particles with silica. Langmuir 19: 6693-6700.

143. Di Corato R, Bigall NC, Ragusa A, Dorfs D, Genovese A, Marotta R, Manna L, Pellegrino T (2011) Multifunctional Nanobeads Based on Quantum Dots and Magnetic Nanoparticles: Synthesis and Cancer Cell Targeting and Sorting. Acs Nano 5: 1109-1121.

144. Xu HY, Aguilar ZP, Yang L, Kuang M, Duan HW, Xiong YH, Wei H, Wang A (2011) Antibody conjugated magnetic iron oxide nanoparticles for cancer cell separation in fresh whole blood. Biomaterials 32: 9758-9765.

145. Bai LL, Du YM, Peng JX, Liu Y, Wang YM, Yang YL, Wang C (2014) Peptide-based isolation of circulating tumor cells by magnetic nanoparticles. Journal of Materials Chemistry B 2: 4080-4088.

146. Yavuz CT, Mayo JT, Yu WW, Prakash A, Falkner JC, Yean S, Cong LL, Shipley HJ, Kan A, Tomson M, Natelson D, Colvin VL (2006) Low-field magnetic separation of monodisperse Fe_3O_4 nanocrystals. Science 314: 964-967.

147. De Las Cuevas G, Faraudo J, Camacho J (2008) Low-gradient magnetophoresis through field-induced reversible aggregation.

Journal of Physical Chemistry C 112: 945-950.

148. Caruso F, Caruso RA, Mohwald H (1998) Nanoengineering of inorganic and hybrid hollow spheres by colloidal templating. Science 282: 1111-1114.

149. Liong M, Lu J, Kovochich M, Xia T, Ruehm SG, Nel AE, Tamanoi F, Zink JI (2008) Multifunctional inorganic nanoparticles for imaging, targeting, and drug delivery. Acs Nano 2: 889-896.

150. Slowing II, Vivero-Escoto JL, Wu CW, Lin VSY (2008) Mesoporous silica nanoparticles as controlled release drug delivery and gene transfection carriers. Advanced Drug Delivery Reviews 60: 1278-1288.

151. De M, Ghosh PS, Rotello VM (2008) Applications of Nanoparticles in Biology. Advanced Materials 20: 4225-4241.

Appendix. Calculation of magnetic force of a single DL M-SiO_2 NP [emu/unit]

- Magnetic force of a single DL M-SiO_2 NP [emu/unit]

  = Magnetic force of DL M-SiO_2 NPs [emu/g] × weight of a single DL M-SiO_2 NP [ng/unit]

  = 5.0 [emu/g] × (9.7×10^{-5}) [ng/unit]

  = 4.9×10^{-13} [emu/unit]

- Weight of a single DL M-SiO_2 NP

  = (Volume of 400 nm DL M-SiO_2 NP [nm^3] – volume of 18 nm Fe_3O_4 [nm^3/unit] × 1200 [unit]) × density of SiO_2 (2.65 g/cm^3) + volume of 18 nm Fe_3O_4 [nm^3/unit] × 1200 [unit] × density of Fe_3O_4 (5.0 g/cm^3)

  = 9.7×10^{-5} [ng]

- Magnetic force of a single Fe_3O_4 NP [emu/unit]

  = Magnetic force of 18 nm Fe_3O_4 [emu/g] × weight of single Fe_3O_4 [g/unit]

  = 60.0 [emu/g] × 1.5×10^{-8} [ng/unit]

  = 9.0×10^{-16} [emu/unit]

- Weight of a single Fe_3O_4 NP

  = Volume of 18 nm Fe_3O_4 [nm^3/unit] × density of Fe_3O_4 (5.0 g/cm^3)

  = 1.5×10^{-8} [ng]

- Magnetic force of a single DL M-SiO_2 NP /magnetic force of a single Fe_3O_4 NP

  = 540

For these calculations, we assumed that; 1) all DL M-SiO_2 NPs were completely spherical in shape, with the same size (r = 200 nm, containing magnetite with r = 9 nm), 2) the DL M-SiO_2 NPs consisted of only silica and Fe_3O_4 NPs, and 3) density of Fe_3O_4 and that of SiO_2 are 5.0 g/cm^3 and 2.65 g/cm^3, respectively.

요 약

강한 형광을 발하는 양자점과 초상자성을 지닌 산화철 나노입자는 의과학 및 생리학 응용연구 분야에서 이미 상당한 이목을 끌고 있다. 하지만 일반적으로 나노물질은 제조 및 보관의 편의상 소수성 물질로 표면이 보호되어있어 표면개질이 선행되지 않으면 생물 응용연구가 불가능하다. 따라서 나노물질의 표면을 의과학 응용에 보다 더 용이한 친수성 물질로 개질하는 기술이 수십년간 다양한 방식으로 개발되어 왔다.

제 1장에서는 실리카 구체 표면에 수백 개의 양자점을 고정한 구조체 (QD-SiO_2 NPs)를 합성하고, 형광 특성 및 세포 관련 생물 연구에 적용시킬 수 있는 지에 대한 잠재성을 확인했다. 합성된 QD-SiO_2 NPs는 단일 양자점 자체의 양자 효율을 안정적으로 유지했기 때문에 단위 입자당 더욱 강한 형광을 방출했으며, 친수성이 있어 세포내 섭취를 통해 쉽게 암세포 내로 도입되었다. 또한 줄기세포의 일종인 인간제대정맥내피세포에 본 물질을 주입하고 세포 분화가 일어난 이후에도, 형광 성질을 잃지 않는 동시에 내피세포의 분화를 방해하지 않았다. 이를 통해 본 물질은 다양한 환경에서의 세포 연구에

표지자로써 적용 가능함을 확인하였다.

제 2장에서는 폴리다이아세틸렌이 표면을 감싸고 있는 양자점 담지 실리카 나노구체 (PDA-QD-SiO_2 NPs)를 합성하고 그 성질을 규명했다. 합성된 PDA-QD-SiO_2 NPs는 표면의 폴리다이아세틸렌과 입자 내부의 양자점 각각의 형광이 스펙트럼의 중첩 및 왜곡 현상 없이 관찰되었다. 열 자극이 가해진 PDA-QD-SiO_2 NPs는 청색에서 적색으로 바뀌었으며 또한 폴리다이아세틸렌 특유의 형광을 관찰할 수 있었다. 또한 변색되지 않은 청색 PDA-QD-SiO_2 NPs와 적색 PDA-QD-SiO_2 NPs을 혼합하여 형광현미경으로 분석한 결과 각각 입자가 잘 영상화되었고 서로 뚜렷하게 구분되었다. 이를 통해 본 PDA-QD-SiO_2 NPs은 여러 표적 물질을 별도의 표지 없이도 동시에의 탐지할 수 있는 잠재성을 가진 것으로 확인했다.

제 3장에서는 초상자성 산화철 나노입자가 중심에 존재하는 양자점 담지 실리카 나노구체 (M-QD-SiO_2 NPs)를 합성하고 그 형광 및 자성을 분석했다. 합성된 M-QD-SiO_2 NPs는 크기가 균일하고 강한 형광과 초상자성을 띄는 것을 확인했다. M-QD-SiO_2 NPs는 모델 암세포인 MDA-MB-231에 쉽게 침투되었으며, 나노입자를 섭취한 세포는 유세포분석기 및 외

부 자기장을 통해 성공적으로 분리되었다. 이 결과를 통해 본 M-QD-SiO_2 NPs의 형광 및 자성을 이용하여 여러 종의 표적 세포를 동시에 분리할 수 있음을 확인하였다.

제 4장에서는 산화철 나노입자가 복층 구조로 이중 고정된 실리카 나노구체 (DL-M-SiO_2 NPs)를 합성하고 그 성질을 규명했다. 합성된 DL-M-SiO_2 NPs는 초상자성을 띄었으며, 외부 자기장에 대하여 매우 효과적인 분리 양상을 보였다. 특히 단일 산화철 나노입자와 단층 실리카 나노구체 (SL-M-SiO_2 NPs)의 경우 외부 자석에 의해 입자가 완전히 회수되지 못하고 일정 구간에서 포화되는 기작을 보였으나 DL-M-SiO_2 NPs의 경우 입자를 완전히 회수할 수 있었다. 또한 바이오틴이 결합된 DL-M-SiO_2 NPs를 이용하여 스트렙타비딘을 비특이적 결합없이 효율적으로 분리했다. 이 결과를 통해 본 DL-M-SiO_2 NPs는 생물 분자를 분리하고 분석하는데 유용함을 확인하였다.

주요어 : 양자점, 초상자성 산화철 나노입자, 실리카 나노입자

학 번 : 2010-20974